J. Fluid Mech. (2012), *vol.* 700, *pp.* 29–62.
doi:10.1017/jfm.2012.89

Two-way coupled stochastic model for dispersion of inertial particles in turbulence

Madhusudan G. Pai†‡ and Shankar Subramaniam†

Department of Mechanical Engineering, Iowa State University, Ames, IA 50011, USA

(Received 29 July 2010; revised 27 January 2012; accepted 16 February 2012;
first published online 18 April 2012)

Turbulent two-phase flows are characterized by the presence of multiple time and length scales. Of particular interest in flows with non-negligible interphase momentum coupling are the time scales associated with interphase turbulent kinetic energy transfer (TKE) and inertial particle dispersion. Point-particle direct numerical simulations (DNS) of homogeneous turbulent flows laden with sub-Kolmogorov size particles report that the time scale associated with the interphase TKE transfer behaves differently with Stokes number than the time scale associated with particle dispersion. Here, the Stokes number is defined as the ratio of the particle momentum response time scale to the Kolmogorov time scale of turbulence. In this study, we propose a two-way coupled stochastic model (CSM), which is a system of two coupled Langevin equations for the fluctuating velocities in each phase. The basis for the model is the Eulerian–Eulerian probability density function formalism for two-phase flows that was established in Pai & Subramaniam (*J. Fluid Mech.*, vol. 628, 2009, pp. 181–228). This new model possesses the unique capability of *simultaneously* capturing the disparate dependence of the time scales associated with interphase TKE transfer and particle dispersion on Stokes number. This is ascertained by comparing predicted trends of statistics of turbulent kinetic energy and particle dispersion in both phases from CSM, for varying Stokes number and mass loading, with point-particle DNS datasets of homogeneous particle-laden flows.

Key words: fluidized beds, gas/liquid flow, multiphase flow

1. Introduction

Particle dispersion and modulation of the ambient carrier-phase turbulence by the dispersing particles have a strong influence on the evolution of a two-phase flow. For instance, as coal particles traverse through an entrained coal gasifier, the rapidly changing ambient gas turbulence disperses the particles. Dispersing coal particles in turn amplify or suppress the turbulence in the ambient gas. The effects of turbulence and coal particle dispersion are therefore intimately coupled. A similar phenomenon occurs when a fuel spray is injected into the combustion chamber of an internal combustion engine or a gas-turbine combustor.

Statistical models that seek to describe turbulent two-phase flows must be capable of capturing the coupled effects of turbulence and particle dispersion. Moreover, the

† Email addresses for correspondence: paim@ge.com, shankar@iastate.edu
‡ Present address: GE Global Research, One Research Circle, Niskayuna, NY 12309, USA.

interactions between the dispersed phase and the carrier phase are multiscale in nature, with the dispersed particles interacting with a range of carrier-phase turbulence time and length scales. Such interactions arise even in simple homogeneous flows, and therefore it is imperative that models reproduce these phenomena and capture these time and length scales in simple flows in order to be predictive in more complex inhomogeneous flows.

An example of a multiscale interaction between the dispersed phase and the carrier phase can be observed even in point-particle direct numerical simulations (DNS) of canonical turbulent flows laden with sub-Kolmogorov size particles, which is the focus of this study. Such interactions manifest in an interesting dependence of the time scales governing interphase turbulent kinetic energy (TKE) transfer and Lagrangian particle velocity autocorrelation, which is a measure of particle dispersion, on Stokes number. It is observed that the time scale for interphase TKE transfer is different from the time scale associated with particle dispersion, and that the trends of these time scales are also different for varying Stokes numbers. Particles with high Stokes number lose energy *faster* than particles with low Stokes number in freely decaying turbulence (Sundaram & Collins 1999). On the other hand, particles with high Stokes number lose correlation with their initial velocities *slower* than particles with low Stokes number in stationary turbulence (Squires & Eaton 1991; Truesdell & Elghobashi 1994; Mashayek *et al.* 1997). The physical explanation is that, with increasing Stokes number, the fluid phase does more work to move the particles around, thereby increasing the interphase transfer of TKE, which in turn results in the draining of energy from the particles to the fluid. However, with increasing Stokes number, the additional dissipation of fluid TKE due to the presence of the particles also increases (and this effect dominates the interphase transfer of TKE), which explains the faster decay of TKE in the fluid phase. Particles with higher Stokes number retain 'memory' of their initial velocities longer, thus explaining the slower decay of the Lagrangian particle velocity autocorrelation.

Experiments also shed light on the multiscale interactions between the dispersed and carrier phases (Snyder & Lumley 1971; Wells & Stock 1983; Groszmann & Rogers 2004). However, in experiments, unlike in the DNS studies, it is difficult to isolate physical mechanisms that affect these multiscale interactions. Models for individual terms in the governing equations for dispersed two-phase flows, such as the interphase TKE, can be tested in isolation by comparing with corresponding terms quantified from DNS. Hence a canonical DNS, such as the ones described earlier, provides useful datasets for comparison with model predictions. Reproducing results from such a canonical two-phase DNS therefore constitutes an important first step in validating multiphase flow turbulence models.

It is noteworthy that two-phase models used in popular Lagrangian–Eulerian (LE) implementations (see e.g. Amsden, O'Rourke & Butler 1989), which evolve the dispersed-phase velocity according to a drag model of the form

$$\frac{\mathrm{d}\boldsymbol{V}_p}{\mathrm{d}t} = \frac{\boldsymbol{U}_f - \boldsymbol{V}_p}{\tau_p} C_d(Re_p) + \boldsymbol{F}_{add}, \tag{1.1}$$

and whose positions evolve according to

$$\frac{\mathrm{d}\boldsymbol{X}_p}{\mathrm{d}t} = \boldsymbol{V}_p, \tag{1.2}$$

are incapable of capturing the observed trends that were noted earlier in the decay of TKE with Stokes number $St_\eta = \tau_p/\tau_\eta$, when tested in the canonical problem of

particle-laden decaying homogeneous turbulence (Pai & Subramaniam 2006). In the above equation, $\boldsymbol{V}_p$ is the instantaneous particle velocity, $\boldsymbol{U}_f$ is the instantaneous gas-phase velocity (also sometimes referred to as the gas-phase velocity 'seen' by the particles), $\tau_p = (\rho_d d_p^2)/(\rho_f 18\nu_f)$ is the particle response time scale, $\boldsymbol{X}_p$ is the particle position and $\boldsymbol{F}_{add}$ represents additional terms that include lift and body forces. The instantaneous gas-phase velocity $\boldsymbol{U}_f$ is decomposed into a mean $\langle \boldsymbol{U}_f \rangle$ and a fluctuating component $\boldsymbol{u}_f'$. Here, ρ_d and ρ_f are the thermodynamic densities of the dispersed phase and fluid phase, respectively, d_p is the particle diameter and ν_f is the kinematic viscosity of the fluid phase. A drag coefficient C_d that depends on the particle Reynolds number Re_p is generally included as shown. In the definition of the Stokes number St_η, $\tau_\eta = (\nu_f/\varepsilon_f)^{1/2}$ is the time scale corresponding to the smallest turbulent eddies, which are characterized by the Kolmogorov length scale η and dissipation rate in the carrier phase ε_f.

The reason for the inability of such models to capture these trends observed in two-phase DNS can be traced to the use of the particle response time scale τ_p in (1.1). It was shown in Pai & Subramaniam (2006) that when τ_p is employed as the time scale for interphase TKE transfer, it is incapable of capturing the multiple time scale interactions of the dispersed phase with the carrier-phase turbulence. When τ_p is replaced by a multiscale interaction time scale, predicted trends of TKE decay from the LE model match DNS results (Pai & Subramaniam 2006), thereby validating the choice of the multiscale interaction time scale as the appropriate time scale for interphase TKE transfer in such statistical models.

The major research effort in modelling turbulent two-phase flows using the LE representation has been directed towards arriving at a suitable model for $\boldsymbol{U}_f$ (see Lu 1995; Chen & Pereira 1997; Mashayek 1999; Pozorski & Minier 1999; Gao & Mashayek 2004; Chagras, Oesterle & Boulet 2005). There is no evidence in the literature of tests conducted with the aforementioned models in canonical two-phase flows such as particle-laden decaying or stationary turbulence to ascertain their capability to simultaneously capture the TKE and dispersion time scales that are observed in DNS datasets. Furthermore, since these models are a prescription for $\boldsymbol{U}_f$ in (1.1), the implied interphase TKE transfer and velocity autocorrelation evolve on the particle response time scale and are therefore incapable of capturing the disparate time scale trends noted earlier.

The primary objective of this work is to propose a two-way coupled Lagrangian model based on stochastic differential equations (SDEs) for dilute particle-laden turbulent flows with non-negligible interphase momentum coupling that reproduces the trend of TKE and particle dispersion statistics with varying Stokes number and mass loading that are observed in DNS. Stochastic Lagrangian models have been successfully employed in single-phase turbulent flows to model the velocity following a fluid particle (Pope 1985). Models that are based on the Langevin equation have the advantage that they are more amenable to analysis than existing LE models based on stochastic white noise (Gosman & Ioannides 1983; Amsden *et al.* 1989). Although Langevin models have been successful in predicting turbulent reactive flows (Pope 1985, 2000), extending such models to two-phase flows is not straightforward. This is because single-phase Langevin models are based on a single time scale (namely the integral time scale) and such models are clearly incapable of simultaneously capturing the disparate time scales of TKE and particle dispersion observed in two-phase DNS.

The two-way coupled stochastic model (CSM) consists of a system of two coupled Langevin equations for the fluctuating velocity in each phase. Unlike the models cited earlier, we do not use (1.1) to evolve the particle velocities, nor do we model the

gas-phase velocity at the particle location $\boldsymbol{U}_f$ as in (1.1). Instead, we propose a model whose implied evolution of statistics models the exact statistics that are obtained from the governing equations for the two-phase flow. This approach is reasonable because this Lagrangian stochastic model does not directly represent fluid particles or dispersed solid particles in a two-phase flow, but rather these are models of notional particles that are consistent with a closure of the underlying probability density function (p.d.f.) description of a two-phase flow – in the context of single-phase flows, see the discussion on stochastic equivalence in Pope (1985). A distinguishing feature of this model is its ability to capture simultaneously the disparate behaviour of TKE and particle velocity autocorrelation evolution with Stokes number that is consistent with DNS datasets. We further demonstrate the capability of the model to be predictive in particle-laden homogeneous shear flows. Such a level of versatility has not been demonstrated by two-phase models available in literature.

The paper begins with a brief review of the statistical representation of two-phase flow that provides the theoretical basis for the proposed model. A general form of the two-way CSM is presented in § 3. Section 4 presents a specific form of CSM as a particular prescription of the drift and diffusion coefficients in the general form of the coupled system. Evolution equations for the TKE and particle velocity autocorrelation that are implied by CSM are then derived. CSM relies on a model for interphase TKE transfer called the equilibrium of energy concept, which is described in § 5. Model constants and the rationale for their choice in the drift and diffusion coefficients are presented in § 6. A description of the DNS datasets that are used to compare predictions from CSM is presented in § 7. This is followed by a detailed comparison of the CSM predictions and DNS datasets in § 8. A detailed appraisal of CSM is then presented in § 9. Section 10 presents a summary that includes important conclusions of the work.

2. Theoretical basis for the coupled stochastic model

We first review salient aspects of the theoretical basis for a coupled stochastic model that is proposed in the context of the Eulerian–Eulerian (EE) statistical formalism. Only details pertinent to the current study are presented, while more details on the theoretical description are provided in Pai & Subramaniam (2009).

The starting point for the EE description is the indicator function I_β. Let the two-phase flow be composed of a carrier phase (such as a gas) and a dispersed phase (such as a solid or liquid). The indicator function $I_\beta(\boldsymbol{x}, t)$ for the βth phase is defined as

$$I_\beta(\boldsymbol{x}, t) = \begin{cases} 1 & \text{if } \boldsymbol{x} \text{ is in phase } \beta \text{ at time } t, \\ 0 & \text{if } \boldsymbol{x} \text{ is not in phase } \beta \text{ at time } t, \end{cases} \tag{2.1}$$

where $\beta = \{f, d\}$, and f represents the carrier phase and d represents the dispersed phase. The instantaneous two-phase velocity field $\boldsymbol{U}(\boldsymbol{x}, t)$ and the instantaneous thermodynamic mass density field $\rho(\boldsymbol{x}, t)$, which are defined in all phases, are vector fields defined at every location $\boldsymbol{x}$ in the flow domain in physical space. One can define a p.d.f. f_U of $\boldsymbol{U}(\boldsymbol{x}, t)$ at location $\boldsymbol{x}$ that can be in either phase β. By conditioning on phase β, an associated phasic p.d.f. $f_{U|I_\beta}$ can be defined as

$$f_{U|I_\beta} = \frac{p_\beta f_U(\boldsymbol{u})}{\alpha_\beta(\boldsymbol{x}, t)}, \tag{2.2}$$

where p_β is the probability that the location $\boldsymbol{x}$ is in phase β conditional on $\boldsymbol{U} = \boldsymbol{u}$. An analogous phasic mass density conditional on phase β can be defined as

$$\mathscr{F}_{\boldsymbol{U}|I_\beta} = \langle \rho I_\beta \mid \boldsymbol{U} = \boldsymbol{u} \rangle f_{\boldsymbol{U}}(\boldsymbol{u}). \tag{2.3}$$

For the zero interphase mass transfer assumed in this study, the transport equation for the phasic mass density (see Pai & Subramaniam 2009, equation (4.13)) is

$$\frac{\partial \mathscr{F}_{\boldsymbol{U}|I_\beta}}{\partial t} + u_k \frac{\partial \mathscr{F}_{\boldsymbol{U}|I_\beta}}{\partial x_k} = -\frac{\partial}{\partial u_k}[\langle A_k|\boldsymbol{u}\rangle \mathscr{F}_{\boldsymbol{U}|I_\beta}], \tag{2.4}$$

where

$$\langle \widetilde{A_k}|\boldsymbol{u}\rangle = \frac{1}{\langle \rho I_\beta \mid \boldsymbol{u}\rangle} \left\langle \rho I_\beta \frac{\mathrm{D}U_k}{\mathrm{D}t} \middle| \boldsymbol{u} \right\rangle \tag{2.5}$$

is the density-weighted expected acceleration conditional on velocity $\boldsymbol{u}$. Under the assumption of constant density in either phase, $\mathscr{F}_{\boldsymbol{U}|I_\beta}$ simplifies to

$$\mathscr{F}_{\boldsymbol{U}|I_\beta} = \rho_\beta p_\beta f_{\boldsymbol{U}} = \rho_\beta \alpha_\beta f_{\boldsymbol{U}|I_\beta}. \tag{2.6}$$

Thus the evolution for the volume fraction-weighted conditional phasic p.d.f. can be written as

$$\frac{\partial(\alpha_\beta f_{\boldsymbol{U}|I_\beta})}{\partial t} + u_i \frac{\partial(\alpha_\beta f_{\boldsymbol{U}|I_\beta})}{\partial x_i} = -\frac{\partial}{\partial u_k}[\langle A_k \mid \boldsymbol{u}\rangle \alpha_\beta f_{\boldsymbol{U}|I_\beta}], \tag{2.7}$$

where the tilde has been removed from the acceleration term to remind us that the unweighted (density-removed) acceleration is equal to the density-weighted counterpart for constant-density two-phase flows. Equation (2.7) shows that the evolution of the volume fraction-weighted Eulerian single-point phasic p.d.f. in velocity space is determined by the conditional acceleration $\langle A_k|\boldsymbol{u}\rangle$. Equation (2.7) governs the evolution of the Eulerian phasic p.d.f. in either phase $\beta = \{f, d\}$. Later we draw the connection between the evolution of $f_{\boldsymbol{U}|I_\beta}$ and the evolution of the p.d.f. corresponding to the coupled stochastic model.

3. General form of a coupled stochastic model for two-phase flows

In its most general form, a coupled stochastic model for the fluctuating velocities in the fluid phase and dispersed phase in a statistically homogeneous two-phase flow system can be written as a matrix system of vector SDEs as

$$\mathrm{d}\begin{pmatrix} \boldsymbol{u} \\ \boldsymbol{v} \end{pmatrix} = \underbrace{\begin{pmatrix} \boldsymbol{a}^{ff} & \boldsymbol{a}^{fd} \\ \boldsymbol{a}^{df} & \boldsymbol{a}^{dd} \end{pmatrix}}_{\boldsymbol{A}} \begin{pmatrix} \boldsymbol{u} \\ \boldsymbol{v} \end{pmatrix} \mathrm{d}t + \underbrace{\begin{pmatrix} \boldsymbol{b}^{ff} & \boldsymbol{b}^{fd} \\ \boldsymbol{b}^{df} & \boldsymbol{b}^{dd} \end{pmatrix}}_{\boldsymbol{B}} \begin{pmatrix} \mathrm{d}\boldsymbol{W}_f \\ \mathrm{d}\boldsymbol{W}_d \end{pmatrix}. \tag{3.1}$$

We have the following in the above coupled system of SDEs.

(i) The velocities $\boldsymbol{u}$ and $\boldsymbol{v}$ are modelled fluctuating velocities in the fluid phase f and dispersed phase d, respectively.

(ii) The matrix denoted $\boldsymbol{A}$ is the drift matrix whose elements $\boldsymbol{a}^{ff}$, $\boldsymbol{a}^{fd}$, $\boldsymbol{a}^{df}$ and $\boldsymbol{a}^{dd}$ have dimension $[\mathrm{T}^{-1}]$. The physical significance of $\boldsymbol{a}^{ff}$ is that it represents the 'friction' coefficient that decays k_f due to dissipation in the turbulent eddies and also accounts for the production term from mean velocity gradients, whereas the physical significance of $\boldsymbol{a}^{dd}$ is that it represents the 'friction' coefficient that

decays the particle TKE through interaction with the range of eddies in fluid turbulence, not just due to Stokes flow around each particle. The cross-coupling terms $\boldsymbol{a}^{fd}$ and $\boldsymbol{a}^{df}$ are zero in a single-point closure model (see discussion that follows).

(iii) The matrix denoted $\boldsymbol{B}$ is the diffusion matrix whose elements $\boldsymbol{b}^{ff}$, $\boldsymbol{b}^{fd}$, $\boldsymbol{b}^{df}$ and $\boldsymbol{b}^{dd}$ have dimension $[\mathrm{LT}^{-3/2}]$. The physical significance of $\boldsymbol{b}^{ff}$ is that it represents the strength of random perturbations to the fluid phase velocity $\boldsymbol{u}^f$ that determines the level of fluid TKE in stationary homogeneous turbulence by the analogue of the fluctuation–dissipation theorem, whereas $\boldsymbol{b}^{dd}$ models the random perturbations to the particle acceleration due to fluid turbulence that are not capable of being represented in the one-point p.d.f. closure. The cross-coupling terms $\boldsymbol{b}^{fd}$ and $\boldsymbol{b}^{df}$ are zero in a single-point closure model (see discussion that follows).

(iv) Finally, $\mathrm{d}\boldsymbol{W}_f$ and $\mathrm{d}\boldsymbol{W}_d$ are independent isotropic Wiener processes. The usual properties of the Wiener process $\langle \boldsymbol{W} \rangle = 0$ and $\langle \boldsymbol{W}(t)\boldsymbol{W}(s) \rangle = \min(t, s)$ hold; furthermore, at any time t and time increment $\mathrm{d}t$, the increment $(\boldsymbol{W}(t+\mathrm{d}t) - \boldsymbol{W}(t))$ is a Gaussian random variable with zero mean and variance dt. Here, $\langle \cdot \rangle$ denotes the mathematical expectation.

A non-zero drift coefficient matrix $\boldsymbol{a}^{fd}$ or $\boldsymbol{a}^{df}$ couples the evolution of $\boldsymbol{u}$ and $\boldsymbol{v}$ and formally leads to particle–fluid velocity correlations such as $\langle \boldsymbol{u} \cdot \boldsymbol{v} \rangle$. However, the single-point limit of such correlations does not have any physical meaning in two-phase flows with finite particle size because fluid particles and dispersed-particle centres cannot coexist at the same physical location. Sundaram & Collins (1999) have shown that the single-point limit of the two-point particle–fluid correlation is identically zero. Owing to this physical constraint, the matrices $\boldsymbol{a}^{fd}$, $\boldsymbol{a}^{df}$, $\boldsymbol{b}^{fd}$ and $\boldsymbol{b}^{df}$ are set to zero:

$$d\begin{pmatrix} \boldsymbol{u} \\ \boldsymbol{v} \end{pmatrix} = \begin{pmatrix} \boldsymbol{a}^{ff} & \boldsymbol{0} \\ \boldsymbol{0} & \boldsymbol{a}^{dd} \end{pmatrix} \begin{pmatrix} \boldsymbol{u} \\ \boldsymbol{v} \end{pmatrix} \mathrm{d}t + \begin{pmatrix} \boldsymbol{b}^{ff} & \boldsymbol{0} \\ \boldsymbol{0} & \boldsymbol{b}^{dd} \end{pmatrix} \begin{pmatrix} \mathrm{d}\boldsymbol{W}_f \\ \mathrm{d}\boldsymbol{W}_d \end{pmatrix}. \tag{3.2}$$

In general, the drift and diffusion coefficients can be functions of the mean velocity gradients in both phases, TKE and viscous dissipation in both phases, in addition to non-dimensional quantities, such as particle Reynolds number, mass loading, volume fraction and dispersed-phase to fluid-phase density ratio. A comparison of the modelled p.d.f. equation or the Fokker–Planck (FP) equations implied by the SDEs in (3.2) with (2.7) reveals the closure approximation in CSM; these FP equations are presented next.

3.1. *Fokker–Planck equation corresponding to the SDEs*

Corresponding to the velocity variables $\boldsymbol{u}$ and $\boldsymbol{v}$ in the system of SDEs given by (3.2), one can define conditional Lagrangian p.d.f.s $f_L^*(\boldsymbol{u}, t \mid \boldsymbol{u}_0, t_0)$ and $f_L^*(\boldsymbol{v}, t \mid \boldsymbol{v}_0, t)$, respectively, where the subscript 0 denotes the initial velocity and initial time. Conditioning these Lagrangian p.d.f.s with the corresponding Eulerian velocity p.d.f. at initial time provides the corresponding Eulerian velocity p.d.f. at later time t. The FP equations for the modelled Eulerian p.d.f. of velocity in the carrier phase $f_U^*(\boldsymbol{u}, t)$ and the dispersed phase $f_V^*(\boldsymbol{v}, t)$ corresponding to the system of stochastic differential equations are (Gardiner 1983; Pope 2000)

$$\frac{\partial}{\partial t} f_U^* + \frac{\partial}{\partial u_i}(a_{ij}^{ff} u_j f_U^*) = \frac{1}{2} \frac{\partial^2}{\partial u_i \partial u_j} [b_{ik}^{ff} b_{jk}^{ff} f_U^*], \tag{3.3}$$

$$\frac{\partial}{\partial t} f_V^* + \frac{\partial}{\partial v_i}(a_{ij}^{dd} v_j f_V^*) = \frac{1}{2}\frac{\partial^2}{\partial v_i \partial v_j}[b_{ik}^{dd} b_{jk}^{dd} f_V^*]. \tag{3.4}$$

The asterisk (*) reminds us that f_U^* is a model corresponding to the exact Eulerian p.d.f. $f_{U|I_\beta}$. The FP equation models the evolution of the p.d.f. $f_{U|I_\beta}$ that is given by (2.7). Generally, the above equation is indirectly solved using a particle method solution. See the Appendix for a description of the particle method solution that is adopted in this study.

In the next section, we explore a form of the drift and diffusion coefficients that is successful in reproducing the decay trends of TKE and velocity autocorrelation that are observed in DNS of dilute particle-laden turbulent flows.

4. Two-way coupled stochastic model

The general form for the coupled stochastic model was presented earlier as a system of SDEs given by (3.2). Since the primary goal of this study is to propose a coupled stochastic model that can simultaneously capture the disparate time scale trends associated with the evolution of TKE and particle velocity autocorrelation observed in DNS of dilute particle-laden turbulent flows, we propose isotropic drift and diffusion coefficients that reproduce these trends. This coupled stochastic model reads

$$\mathrm{d}u_i = -\left(A(t)\delta_{ij} + \frac{\partial \langle U_i \rangle}{\partial x_j}\right) u_j \,\mathrm{d}t + B(t)\delta_{ij}\,\mathrm{d}W_{f_j}, \tag{4.1}$$

$$\mathrm{d}v_i = -\left(C(t)\delta_{ij} + \frac{\partial \langle V_i \rangle}{\partial x_j}\right) v_j \,\mathrm{d}t + D(t)\delta_{ij}\,\mathrm{d}W_{p_j}, \tag{4.2}$$

where

$$A(t) = \left[\frac{1}{2\tau_1} + \left(\frac{1}{2} + \frac{3}{4}C_0\right)\frac{\varepsilon_f}{k_f}\right], \tag{4.3}$$

$$B(t) = \left[C_0\varepsilon_f + \frac{2}{3}\frac{k_f}{\tau_1} + \frac{2}{3}\left(\frac{k_f^e - k_f}{\tau_2}\right)\right]^{1/2}, \tag{4.4}$$

$$C(t) = \frac{1}{2\tau_3}, \tag{4.5}$$

$$D(t) = \left[\frac{2}{3}\frac{k_d}{\tau_3} + \frac{2}{3}\left(\frac{k_d^e - k_d}{\tau_4}\right)\right]^{1/2}. \tag{4.6}$$

For the homogeneous test cases studied in this work, and for the drift coefficients to be isotropic, the mean velocity gradient in each phase must be constant. Thus, for a mean shear in the 1–3 direction, $\partial\langle U_i\rangle/\partial x_j = \partial\langle V_i\rangle/\partial x_j = \mathscr{S}\delta_{i1}\delta_{j3}$, where $\mathscr{S}$ is the constant imposed mean shear and δ_{ij} is the Kronecker delta. In the above equation, τ_1 and τ_3 are time scales that appear in the drift coefficients, while τ_2 and τ_4 are time scales that appear in the diffusion coefficients of each SDE; the importance of these time scales will become clear shortly. The TKE in the dispersed phase is denoted k_d with a superscript 'e' to denote 'equilibrium' values (the same holds for the TKE in the fluid phase k_f). The gas-phase dissipation enhanced by the presence of the dispersed phase is denoted ε_f. The rationale behind this particular choice of the drift and diffusion coefficients and the reason for the use of the term 'equilibrium' are explained in the next section.

The fluid-phase SDE can be viewed as an extension of the simplified Langevin model (SLM) (Haworth & Pope 1986; Pope 2000) to two-phase flows, but with an important difference being the introduction of drift and diffusion time scales that are different from each other. Additional terms that represent interphase interactions have been included. In this model, the coupling between the two phases is only through mean fields like TKE (k_f and k_d) and ε_f, and not explicitly through u_i and v_i, for reasons outlined earlier.

The reason to choose SLM as a basis for CSM is manifold. SLM performs well in the context of single-phase flows (Pope 2000), where for stationary turbulence the Lagrangian integral time scale matches well with DNS results (Yeung & Pope 1989). The form of the second-order structure function as implied by SLM is linear in time separation, which is consistent with Kolmogorov's hypotheses. In single-phase homogeneous shear flows, SLM is a reasonable model for the Lagrangian velocity of a fluid particle (Pope 2002). However, in homogeneous shear flows, when the Reynolds stresses and the Lagrangian integral time scale from DNS (Sawford & Yeung 2001) are employed to arrive at the implied diffusion coefficient in SLM, Pope (2002) does find that this coefficient is significantly anisotropic; although it is not clear if the anisotropy is an effect of the low-Reynolds-number regime studied in the DNS. A value of $C_0 = 3.4$ has also been used by Pope in the same study, with better agreement of model predictions with DNS results, than with $C_0 = 2.1$.

In this study, the primary emphasis is to match trends of important two-phase statistics in canonical two-phase flows for varying non-dimensional parameters, such as Stokes number and mass loading, with those observed in DNS. For the purposes of this study, we use the simplest form of the single-phase Langevin model as the single-phase limit of CSM with $C_0 = 2.1$. Recent model developments to such Langevin models can be incorporated into the two-phase flow model proposed in this paper.

4.1. *Implied evolution equation for the Reynolds stresses*

The evolution equations of key statistics in a two-phase flow as implied by CSM are now derived. Following a standard procedure (see e.g. Pope 2000), the evolution equations for the phasic Reynolds stresses implied by CSM are obtained as

$$\frac{\mathrm{d}}{\mathrm{d}t}\langle u_i u_j\rangle = -2A(t)\langle u_i u_j\rangle - \left(\langle u_k u_j\rangle \mathscr{S}\delta_{1i}\delta_{k3} + \langle u_i u_k\rangle \mathscr{S}\delta_{j1}\delta_{k3}\right) + B\,(t)^2\,\delta_{ij}, \tag{4.7}$$

$$\frac{\mathrm{d}}{\mathrm{d}t}\langle v_i v_j\rangle = -2C(t)\langle v_i v_j\rangle - \left(\langle v_k v_j\rangle \mathscr{S}\delta_{1i}\delta_{k3} + \langle v_i v_k\rangle \mathscr{S}\delta_{j1}\delta_{k3}\right) + D\,(t)^2\,\delta_{ij}, \tag{4.8}$$

where the second term enclosed in parentheses on the right-hand side of the above equations represents the production due to mean velocity gradients.

4.2. *Implied evolution equations for the TKE*

Contracting like indices in (4.7) and (4.8) results in the evolution equations for the TKE in the fluid phase, defined as $k_f = (1/2)\langle u_i u_i\rangle$, and the TKE in the dispersed phase, defined as $k_d = (1/2)\langle v_i v_i\rangle$, respectively:

$$\frac{\mathrm{d}k_f}{\mathrm{d}t} = -2A(t)k_f - \langle u_3 u_1\rangle \mathscr{S} + \frac{3}{2}B\,(t)^2, \tag{4.9}$$

$$\frac{\mathrm{d}k_d}{\mathrm{d}t} = -2C(t)k_d - \langle v_3 v_1\rangle \mathscr{S} + \frac{3}{2}D\,(t)^2\,. \tag{4.10}$$

Simplifying the above equation using the prescribed form of the drift and diffusion coefficients results in

$$\frac{\mathrm{d}k_f}{\mathrm{d}t} = -\frac{k_f - k_f^e}{\tau_2} - \langle u_3 u_1 \rangle \mathscr{S} - \varepsilon_f, \tag{4.11}$$

$$\frac{\mathrm{d}k_d}{\mathrm{d}t} = -\frac{k_d - k_d^e}{\tau_4} - \langle v_3 v_1 \rangle \mathscr{S}. \tag{4.12}$$

The first term on the right-hand side of the above equations represents the modelled interphase TKE transfer term (Xu & Subramaniam 2006; Pai & Subramaniam 2007), while the second term represents the production due to the constant mean velocity gradient. The effects of viscous dissipation on the fluid phase TKE manifest themselves in the ε_f term of (4.11). We assume in this study that collisional dissipation in the dispersed phase is negligible owing to the dilute two-phase flow, and hence a dissipation term does not appear in (4.12) (see § 5 for further discussion on this aspect). Note that τ_2 and τ_4 are the time scales governing the evolution of the interphase TKE transfer. For zero mean velocity gradient (such as in the context of homogeneous, isotropic particle-laden turbulence), the evolution equations for the TKE in each phase given by (4.11) and (4.12) simplify to

$$\frac{\mathrm{d}k_f}{\mathrm{d}t} = -\frac{k_f - k_f^e}{\tau_2} - \varepsilon_f, \tag{4.13}$$

$$\frac{\mathrm{d}k_d}{\mathrm{d}t} = -\frac{k_d - k_d^e}{\tau_4}. \tag{4.14}$$

4.3. *Implied Lagrangian velocity autocorrelation*

The Lagrangian velocity autocorrelation in phase β, denoted $\rho_{\beta_{ij}}(t, s)$, is defined (for $t > t_0$) as

$$\rho_{\beta_{ij}}(t, s) = \frac{\langle \gamma_i(t)\gamma_j(t+s)\rangle}{(\langle \gamma_i(t)\gamma_i(t)\rangle)^{1/2}\langle \gamma_j(t+s)\gamma_j(t+s)\rangle^{1/2}} \tag{4.15}$$

(no summation is implied over repeated indices), where γ stands for either u or v. The Lagrangian autocorrelation is simply a normalized autocovariance, and gives a measure of how quickly the phase velocity loses correlation with its value at some earlier time. In stationary (weak stationarity in particle-laden flows can be ascertained by observing the evolution of statistics such as TKE in either phase) particle-laden turbulence, $\rho_{\beta_{ij}}$ depends only on the *separation* time s, and not on t:

$$\rho_{\beta_{ij}}(s) = \frac{\langle \gamma_i(t_0)\gamma_j(t_0+s)\rangle}{(\langle \gamma_i(t_0)\gamma_i(t_0)\rangle)^{1/2}\langle \gamma_j(t_0+s)\gamma_j(t_0+s)\rangle^{1/2}}, \tag{4.16}$$

where t_0 can be any initial time after the system reaches stationarity. In statistically non-stationary flows (such as particle-laden decaying turbulence), the velocity autocorrelation also depends on the time t_0. Evolution equations for the fluid-phase velocity autocovariance and the dispersed-phase velocity autocovariance can be derived as

$$\frac{\mathrm{d}}{\mathrm{d}t}\langle u_i(t_0)u_j(t)\rangle = -\left[\frac{1}{2\tau_1} + \left(\frac{1}{2} + \frac{3}{4}C_0\right)\frac{\varepsilon_f}{k_f}\right]\langle u_i(t_0)u_j(t)\rangle - \mathscr{S}\delta_{j1}\delta_{k3}\langle u_i(t_0)u_k(t)\rangle \tag{4.17}$$

and

$$\frac{\mathrm{d}}{\mathrm{d}t}\langle v_i(t_0)v_j(t)\rangle = -\frac{1}{2\tau_3}\langle v_i(t_0)v_j(t)\rangle - \mathscr{S}\delta_{j1}\delta_{k3}\langle v_i(t_0)v_k(t)\rangle, \tag{4.18}$$

respectively.

For homogeneous particle-laden turbulent flows in the absence of mean velocity gradients, the evolution equations for the velocity autocovariance in each phase given by (4.17) and (4.18) simplify to

$$\frac{\mathrm{d}}{\mathrm{d}t}\langle u_i(t_0)u_j(t)\rangle = -\left[\frac{1}{2\tau_1} + \left(\frac{1}{2} + \frac{3}{4}C_0\right)\frac{\varepsilon_f}{k_f}\right]\langle u_i(t_0)u_j(t)\rangle, \tag{4.19}$$

$$\frac{\mathrm{d}}{\mathrm{d}t}\langle v_i(t_0)v_j(t)\rangle = -\frac{1}{2\tau_3}\langle v_i(t_0)v_j(t)\rangle, \tag{4.20}$$

where, for stationary turbulence, the $\frac{1}{2}$ in the parentheses in (4.19) is dropped.

A striking feature of CSM is revealed when observing (4.13), (4.14), (4.19) and (4.20): only one of the four time scales τ_1, τ_2, τ_3 and τ_4 appears in each of the four equations. Each of these time scales can potentially be modelled to behave independently of the others. However, as we will see later, in order to represent the correct physics of the two-phase flow, these time scales are not entirely independent. Still, we find that using CSM, the evolution of TKE can be modelled to behave *differently* from the evolution of the velocity autocovariance. It is therefore possible to incorporate the capability of capturing the disparate time scale trends observed in two-phase DNS into CSM.

The equilibrium energies k_f^e and k_d^e in (4.1) and (4.2) are related, as shown next, and so the evolutions of k_f and k_d are coupled through these terms. The proposed form of the TKE evolution equations (4.11) and (4.12) and the relation between the equilibrium energies is based on the equilibration of energy (EoE) model for interphase TKE transfer. We briefly review this model next.

5. Equilibration of energy concept

To explain the EoE concept, which was proposed by Xu & Subramaniam (2006), the following model system of equations for the evolution of TKE in a dilute homogeneous two-phase flow system are assumed to hold:

$$\frac{\mathrm{d}e_f}{\mathrm{d}t} = \Pi_{k_f} - \rho_f\alpha_f\varepsilon_f, \tag{5.1}$$

$$\frac{\mathrm{d}e_d}{\mathrm{d}t} = \Pi_{k_d}, \tag{5.2}$$

where $\Pi_{k_f} = (e_f^e - e_f)/\tau_\pi$ and $\Pi_{k_d} = (e_d^e - e_d)/\tau_\pi$ are the interphase TKE transfer terms. Here, τ_π is the interphase TKE transfer time scale, $e_f = \rho_f\alpha_f k_f$ and $e_d = \rho_d\alpha_d k_d$ are the *specific* carrier-phase and dispersed-phase energies, respectively, and $e_f^e = \rho_f\alpha_f k_f^e$ and $e_d^e = \rho_d\alpha_d k_d^e$ are the equilibrium *specific* TKEs in the carrier phase and dispersed phase, respectively. Collisions among particles are assumed to be elastic and hence no dissipation is considered in the dispersed phase. There is an implicit assumption of sub-Kolmogorov size particles in the above equations. This is because large particles can shed wakes that can in turn lead to an increase in TKE of the carrier phase. Increase in carrier flow TKE due to particle wakes is considered negligible in this study.

The EoE concept states that, if

$$\frac{\mathrm{d}e_m}{\mathrm{d}t} = -\rho_f \alpha_f \varepsilon_f + \mathscr{F}_f = 0, \tag{5.3}$$

where $\mathscr{F}_f$ is the external artificial forcing required to balance the dissipation in order to maintain $\mathrm{d}e_m/\mathrm{d}t = 0$, then the specific dispersed-phase TKE and specific fluid-phase TKE evolve to their respective equilibrium values. In the above equation, $e_m = \rho_m k_m = e_f + e_d = \rho_f \alpha_f k_f + \rho_d \alpha_d k_d$ is the mixture energy in the two-phase flow system and ρ_m is the mixture density defined as $\rho_m = \rho_d \alpha_d + \rho_f \alpha_f$. The dissipation in the carrier phase ε_f is assumed to consist of (not necessarily a sum of contributions): (i) a part due to the single-phase dissipation in the bulk fluid that is present even in the absence of particles, and (ii) an energy loss due to the drag at the particle surfaces (this contribution includes the energy loss due to the velocity gradients in the boundary layers around the dispersed particles). Implicit in (5.3) is the assumption that $\Pi_{k_f} = -\Pi_{k_d}$, which implies that the interphase TKE transfer is conservative. This assumption has been shown to hold for rigid particle-laden turbulent flows (Xu & Subramaniam 2007).

Equilibrium values of the specific fluid-phase TKE e_f^e and specific dispersed-phase TKE e_d^e are determined by a model parameter C_k, which is defined as

$$\frac{e_d^e}{e_m} = C_k \quad \text{or} \quad \frac{e_f^e}{e_m} = 1 - C_k. \tag{5.4}$$

Since C_k represents the fraction of the specific mixture energy present in the dispersed phase at equilibrium, it must lie between zero and unity.

An implicit dependence of C_k on mass loading ϕ of the two-phase system can be ascertained by rewriting (5.4) as

$$C_k = \frac{\rho_d \alpha_d k_d^e}{\rho_m k_m} = \frac{\rho_d \alpha_d k_d^e}{\rho_f \alpha_f k_f^e + \rho_d \alpha_d k_d^e} = \frac{\phi k_d^e / k_f^e}{1 + \phi k_d^e / k_f^e}, \tag{5.5}$$

where ϕ is the mass loading of the two-phase system. The model parameter C_k can also depend on other non-dimensional quantities such as Stokes number St_η, particle Reynolds number Re_d, initial k_d/k_f ratio, the ratio of the particle diameter d_p to the Kolmogorov length scale η, and the dispersed-phase volume fraction α_d.

For a constant mass loading ϕ, decreasing Stokes number should drive the dispersed-phase equilibrium TKE closer to the fluid-phase equilibrium TKE, and in the limit of zero Stokes number, the two equilibrium energies should match. This observation imposes a constraint on C_k in the limiting case of zero Stokes number, and from (5.5) we get

$$C_k|_{St_\eta = 0} = \frac{\phi}{1 + \phi}. \tag{5.6}$$

The EoE concept can be extended to the case where the turbulence decays in time (no artificial forcing of the mixture energy in the two-phase flow system). However, the system of equations (cf. (5.1)–(5.2)) needs to be augmented by an equation for the dissipation rate evolution (details can be found in Xu & Subramaniam (2006), where the extension of the EoE concept to inhomogeneous flows in the context of EE statistical representation of two-phase flows is also presented):

$$\frac{\mathrm{d}\varepsilon_f}{\mathrm{d}t} = -C_{\varepsilon 2} \frac{\varepsilon_f^2}{k_f} + C_s \frac{\varepsilon_f}{k_f} \left(\frac{k_f^e - k_f}{\tau_\pi} \right) - C_{\varepsilon 1} \langle u_i u_j \rangle \frac{\partial \langle U_i \rangle}{\partial x_j} \frac{\varepsilon_f}{k_f}, \tag{5.7}$$

where ε_f is the fluid-phase dissipation evolving according to a modified single-phase ε equation with the production term due to mean velocity gradients. This dissipation rate equation is similar to that proposed by Simonin (1996*a*,*b*), except for the term due to interphase TKE transfer, which arises from the EoE model. Note that the mean velocity gradient in the third term on the right-hand side of (5.7) is assumed to be a constant as noted earlier on account of homogeneity. The model constants $C_{\varepsilon 1}$ and $C_{\varepsilon 2}$ are to be 1.44 and 1.92, respectively. These model constants are identical to those employed in EE models that are described in Simonin (1996*a*,*b*) and Xu & Subramaniam (2006). The constant C_3 is equal to 3, as this value provided the best agreement with DNS datasets in our tests. As more DNS datasets that quantify the interphase momentum transfer term and the time scale of its evolution in the dissipation evolution become available, this constant could change.

Note that, in non-stationary particle-laden turbulent flows, C_k can be expected to be a function of time. Furthermore, in such flows, the equilibrium energies in (5.4) have to be interpreted as notional target values rather than as a stationary equilibrium state of the two-phase flow, since the equilibrium energies are a function of the mixture mean energy, which is itself a function of time in non-stationary particle-laden flows.

6. Model constants in CSM

6.1. *Specification of* C_k

The EoE model parameter C_k defined in (5.5) represents the ratio of specific TKE in the dispersed phase to that in the two-phase mixture. As noted in § 5, C_k can depend on mass loading ϕ, Stokes number St_η, particle Reynolds number Re_d, initial k_d/k_f ratio and the dispersed-phase volume fraction α_d corresponding to a two-phase flow. The particle Reynolds numbers considered in this study are of $O(1)$, dispersed-phase volume fractions are of $O(10^{-3})$ and the initial k_d/k_f ratio is of $O(1)$. Hence, the dependence of C_k on these parameters is neglected in this study. However, if the above non-dimensional parameters vary by an order of magnitude, we expect that the dependence of C_k on these parameters will need to be taken into account.

The dependence of C_k on mass loading and Stokes number St_η is accounted for in this study. Hereafter, 'Stokes number' refers to St_η, the Stokes number based on the Kolmogorov time scale, unless noted otherwise. Since the ratio of the equilibrium TKEs k_d^e/k_f^e (cf. (5.5)) is not known *a priori*, a model for C_k is required. The following model for C_k is proposed:

$$C_k = \frac{\phi}{1+\phi+St_\eta}. \tag{6.1}$$

Note that this specification obeys the correct limiting behaviour of C_k as $St_\eta \to 0$ (cf. (5.6).) There could be other forms of C_k that are more elegant, such as a separable form, $C_k = f(\phi)g(St_\eta)$. In order to improve the model for C_k, datasets from carefully controlled DNS of particle-laden turbulent flows that report the fraction of the mixture energy in each phase are required. Also, the DNS should quantify the effect of non-dimensional parameters in a two-phase flow system, as noted earlier, on the fraction of specific TKE in each phase. To the knowledge of the authors, no such DNS datasets are as yet available in the literature.

6.2. *Drift time scales in CSM*

The form of the drift time scales τ_1 and τ_3 in (4.1) and (4.2), respectively, is now developed based on how we expect the system of SDEs to behave in limiting cases.

6.2.1. *Zero Stokes number limit*

As noted in the introduction, in the limit of zero Stokes number, the dispersed particles respond immediately to the surrounding fluid. In this limit, the fluid-phase velocity autocovariance and the dispersed-phase velocity autocovariance must match. Therefore, we require that, in the limit of vanishing Stokes number, the time scale τ_3 in (4.18) should tend to τ_1, the characteristic time scale of the *fluid* velocity autocovariance decay in (4.17).

A simple specification that satisfies this requirement for τ_3 is

$$\frac{1}{\tau_3} = 2\left[\frac{1}{2\tau_1} + \left(\frac{1}{2} + \frac{3}{4}C_0\right)\frac{1}{\tau}\right]\frac{1}{1 + St_\eta C_3}, \tag{6.2}$$

where $C_3 = 0.1$ is a model constant whose value is chosen to achieve the best agreement with DNS datasets described in § 7. Although there is no explicit dependence of the time scale τ_3 on mass loading ϕ, we show next that the dependence on ϕ does appear through the time scale τ_1. The time scale τ_3 obeys the limiting behaviour as $St_\eta \to 0$, *viz.*

$$\lim_{St_\eta \to 0}\left\{\left[\frac{1}{2\tau_1} + \left(\frac{1}{2} + \frac{3}{4}C_0\right)\frac{1}{\tau}\right]\frac{1}{1 + St_\eta C_3}\right\} = \frac{1}{2\tau_1} + \left(\frac{1}{2} + \frac{3}{4}C_0\right)\frac{1}{\tau}. \tag{6.3}$$

Currently, particle velocity autocorrelation data for large Stokes number (say, $St_\eta > 10$) are not available from DNS or experiments that can help to determine the behaviour of τ_3 in the large St_η limit. Furthermore, there is a limit to which datasets from DNS that use the point-particle approximation can be used for model validation. It can be shown that, if the density ratio ρ_d/ρ_f is of $O(1000)$, then the maximum value of St_η for which the point-particle approximation is valid is around 10 (see the analysis in L'vov, Ooms & Pomyalov 2003). It is surmised that this upper limit of St_η is also the upper limit for the validity of CSM, although this needs to be validated by comparison with DNS. Nevertheless, we do assess the behaviour of CSM in the limit $St_\eta \to \infty$ in § 9.

6.2.2. *Zero mass loading limit*

In the limit of zero mass loading, the effect of the dispersed phase on the fluid-phase momentum is negligible, and this corresponds to the limit of one-way coupling. Regardless of the Stokes number, the fluid time scales remain unaffected by the presence of the dispersed phase and are identical to those seen in a single-phase flow. In this limit, the time scale τ_1, which essentially represents the modification to the fluid velocity autocorrelation time scale due to the presence of dispersed phase, should tend to zero. Therefore, we require that the drift time scale in (4.1) should approach the specification for the single-phase SLM (Pope 2000).

Using available data from DNS of particle-laden flows (Truesdell & Elghobashi 1994; Ahmed & Elghobashi 2001), we propose the following form of τ_1:

$$\frac{1}{\tau_1} = \frac{C_1 \phi St_\eta}{\tau}, \tag{6.4}$$

where C_1 is a model constant ($C_1 = 2.5$). This specification obeys the correct limiting behaviour as $\phi \to 0$, *viz.*

$$\lim_{\phi \to 0}\left[\frac{1}{2\tau_1} + \left(\frac{1}{2} + \frac{3}{4}C_0\right)\frac{1}{\tau}\right] = \left(\frac{1}{2} + \frac{3}{4}C_0\right)\frac{1}{\tau}. \tag{6.5}$$

For constant mass loading, and in the limit $St_\eta \to 0$, the dispersed-phase velocity autocorrelation behaviour is identical to that of the fluid phase. In this limit, the time scale for the decay of velocity autocorrelation is the single-phase velocity autocorrelation decay time scale. Hence, the above specification of τ_1 ensures that, as $St_\eta \to 0$, the time scale $1/\tau_1 \to 0$.

6.3. *Diffusion time scales in CSM*

The time scales τ_2 and τ_4 govern the evolution of TKE in each phase (cf. (4.13) and (4.14)). In accordance with the EoE concept, and to introduce the capability of capturing the multiscale nature of a turbulent two-phase mixture into CSM, the time scales τ_2 and τ_4 are chosen to be equal to $\tau_\pi = \langle \tau_{int} \rangle / C_\pi$, where $\langle \tau_{int} \rangle$ is a multiscale interaction time scale for interphase TKE transfer proposed by Pai & Subramaniam (2006). It was shown in that study that the new time scale accurately captures the dependence of the interphase TKE transfer on St_η. This time scale has been successfully employed in the context of EE two-phase turbulence modelling by Xu & Subramaniam (2006). The constant C_π is chosen to be 1.0 in this study. Details on the development of the time scale are given in Pai & Subramaniam (2006) and Xu & Subramaniam (2006). Only important results are reviewed here for the sake of completeness.

In the spectral description of particle–turbulence interaction, a dispersed particle interacts with a range of eddies, which in turn corresponds to a range of wavenumbers in the fluid-phase TKE spectrum. One may define a Stokes number St_κ as the ratio of the particle response time scale τ_p to the time scale τ_κ corresponding to the eddies of wavenumber κ. Some eddies (say, type A) in this range have a time scale such that $St_\kappa > 1$, while the others (say, type B) in this range have a time scale such that $St_\kappa < 1$. The hypothesis behind the multiscale interaction time scale is that the time scale of interphase energy transfer is not the same when the particle interacts with the two types of eddies. Let us suppose that the particle is interacting with eddies of type A. Since $St_\kappa > 1$ for these eddies, the time scale τ_κ over which the eddy loses energy is *smaller* than the time scale τ_p over which the particle loses energy. In other words, the larger particle response time scale limits the transfer of energy between the particle and the eddy. Consequently, the time scale for interphase energy transfer at this scale is determined more by the particle response time scale. Now let us consider the case where the same particle interacts with an eddy of type B. Since $St_\kappa < 1$, the time scale τ_κ over which the eddy loses energy is *greater* than the time scale τ_p over which the particle loses energy. In other words, the larger eddy time scale limits the transfer of energy between the particle and the eddy. Consequently, the energy transfer between the particle and the eddy at this scale is determined more by the eddy time scale τ_κ. Thus, the effective time scale for particle–turbulence interaction is obtained by integrating the effects of the two wavenumber ranges identified above over the energy spectrum of fluid-phase turbulence in the two-phase flow. The multiscale interaction time scale $\langle \tau_{int} \rangle$ presented here is a single-point analogue of the above spectral model.

Let $\boldsymbol{u}$ be a model for the Eulerian gas-phase velocity (such as the one given by (4.1)). If z is the sample-space variable corresponding to the random variable $Z = |\boldsymbol{u}|$, the multiscale interaction time scale $\langle \tau_{int} \rangle$ is given as

$$\langle \tau_{int} \rangle = \int_{|\boldsymbol{u}|^*}^{\infty} \langle \tau_{int} \mid Z = z \rangle f_Z(z)\, \mathrm{d}z + \int_0^{|\boldsymbol{u}|^*} \tau_p f_Z(z)\, \mathrm{d}z, \tag{6.6}$$

where $f_Z(z)$ the p.d.f. of Z. The conditional mean $\langle \tau_{int} \mid z \rangle$ is given as

$$\langle \tau_{int} \mid z \rangle = St_l(\tau_p - \tau) + \tau \tag{6.7}$$

for $|\boldsymbol{u}|^* \leqslant |\boldsymbol{u}| \leqslant \infty$, while $\langle \tau_{int} \mid z \rangle = \tau_p$ for $0 \leqslant |\boldsymbol{u}| \leqslant |\boldsymbol{u}|^*$. Here, a Stokes number valid in the inertial range is given as

$$St_l = \frac{\tau_p}{\tau_l}, \tag{6.8}$$

where τ_l is computed as

$$\tau_l = \frac{|\boldsymbol{u}|^2}{\varepsilon_f}. \tag{6.9}$$

In order to complete the specification of the multiscale interaction time scale, the p.d.f. of $|\boldsymbol{u}|$ is required. Using (4.1) the p.d.f. of $\boldsymbol{u}$ can be computed directly from the solution. However, if $\boldsymbol{u}$ is assumed to obey a joint normal distribution with zero mean and covariance $\sigma_f^2 \delta_{ij}$, where $\sigma_f^2 = (2/3)k_f$ and δ_{ij} is the Kronecker delta, as is done in recent studies (Pai & Subramaniam 2006; Xu & Subramaniam 2006), then the p.d.f. of $Z = |\boldsymbol{u}|$ is

$$f_Z(z) = \sqrt{\frac{2}{\pi}} \frac{1}{\sigma_f^3} z^2 \mathrm{e}^{-z^2/2\sigma_f^2}. \tag{6.10}$$

As noted above, (6.9) is based on an inertial sub-range scaling where eddies have a characteristic length scale l. The Stokes number St_l defined in (6.8) using the characteristic length scale is the single-point analogue of St_κ. For a value of $St_l > 1$, the particle responds slowly to the eddies and the time scale of energy transfer is influenced more by the particle response time τ_p. On the other hand, if $St_l < 1$, the particle responds immediately to the flow, and the time scale of energy transfer is influenced more by the eddy turnover time scale τ. Thus, the p.d.f. of $|\boldsymbol{u}|$ (see figure 1 for a Gaussian $\boldsymbol{u}$) can be divided into two regions – one that represents $St_l > 1$ and the other that represents $St_l < 1$, with $|\boldsymbol{u}|^*$ representing the transition between the two regions at $St_l = 1$. Thus, $|\boldsymbol{u}|^*$ is uniquely determined by the relation $(|\boldsymbol{u}|^*)^2 = \tau_p \varepsilon_f$.

It is interesting to note that (6.6) has the correct behaviour for limiting values of St_l and $|\boldsymbol{u}|^*$. In the limit $|\boldsymbol{u}|^* \to 0$, there are no eddies in the system with $St_l > 1$. The dispersed particles are simply convected by the flow and the correct time scale for interphase TKE transfer in this limit is τ. In the limit $|\boldsymbol{u}|^* \to \infty$, practically all the eddies in the system satisfy $St_l > 1$, which implies that there are no eddies energetic enough to convect the particles. The correct time scale for interphase TKE transfer in this limit is the particle response time scale τ_p.

7. DNS datasets for model validation

Several researchers (Mashayek *et al.* 1997; Boivin, Simonin & Squires 1998; Sundaram & Collins 1999) have performed point-particle DNS of particle-laden homogeneous turbulent flows for density ratios in the range $\rho_d/\rho_f \sim O(1000)$ and particle size ratios in the range $d/\eta < 1$, which is the parameter range explored in this study. For this density and particle size ratio, the point-particle assumption is generally invoked in such DNS, which implies that the dispersed particles are represented as point sources in the fluid-phase momentum equation. In this parameter range, the only significant contribution to the particle acceleration is through particle

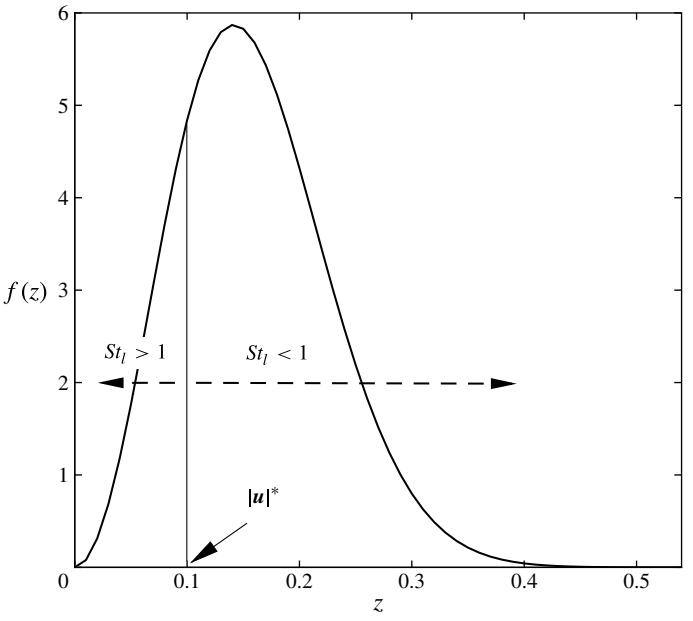

FIGURE 1. A schematic probability density function of $|\boldsymbol{u}|$ that is used in the derivation of the multiscale interaction time scale $\langle \tau_{int} \rangle$. The sample space variable corresponding to $|\boldsymbol{u}|$ is z.

drag. Such DNS directly calculate the contribution to the fluid-phase dissipation ε_f due to viscous dissipation in the bulk. The dissipation of fluid-phase TKE due to the presence of particles is modelled. However, this contribution does not include the additional dissipation due to the velocity gradients in the boundary layer around the dispersed particles. (See Xu & Subramaniam (2007), where the dissipation rate in a point-particle DNS is contrasted with the dissipation rate in particle-resolved two-phase DNS.) Particle-resolved DNS of particle-laden flows are becoming commonplace with advances in numerical techniques and access to increasing computational power, but it is still prohibitively expensive to simulate realistic turbulence Reynolds numbers (Xu & Subramaniam 2010). Recent advances in numerical techniques for particle-laden flows, such as the immersed boundary methods (Yusof 1996; Fadlun *et al.* 2000), arbitrary LE method (Hu, Zhu & Patankar 2001) and lattice-Boltzmann methods (Ten Cate *et al.* 2004), possess the capability of quantifying the increased dissipation in the carrier phase due to the boundary layers surrounding the particles, in addition to the modulation of the carrier-phase TKE by the dispersed particles. No such DNS datasets are as yet available to validate CSM in the parameter range explored in this study. Nevertheless, we do expect that the point-particle DNS qualitatively capture the correct trends in key statistics, such as TKE and particle velocity autocorrelation, with varying Stokes number and mass loading.

In this study, two important test cases are considered. The first is particle-laden freely decaying turbulence, which is an important canonical two-phase problem and a necessary test for two-phase models. This test problem is especially important since models based on the momentum response time scale fail to capture accurate trends of TKE decay with varying Stokes number that are observed in DNS (Pai & Subramaniam 2006). In this study, we ascertain if CSM can capture these trends. Since dispersion and dynamics (interphase TKE transfer) are two coupled phenomena

DNS dataset	Characteristics	Purpose of comparison
SC	Two-way coupled, homogeneous decaying isotropic turbulence	Evolution of k_f and k_d
TE	Two-way coupled, homogeneous decaying isotropic turbulence	Evolution of dispersed-phase velocity autocorrelation
AE-1	Two-way coupled, homogeneously sheared non-stationary and non-isotropic turbulence	Evolution of k_f and k_d
AE-2	One-way coupled, homogeneously sheared non-stationary and non-isotropic turbulence	Evolution of fluid-phase and dispersed-phase velocity autocorrelation

TABLE 1. Summary of the DNS datasets used in this study.

in any two-phase flow, we also investigate if CSM can capture the trends of velocity autocorrelation (which characterizes dispersion) with varying particle inertia. Another important test case is particle-laden homogeneous shear, where there is an interplay of production due to mean velocity gradients, interphase TKE transfer and carrier-phase dissipation. We compare CSM predictions for the evolution of TKE and particle dispersion in the homogeneous shear test case with DNS results. Particle-laden stationary turbulence is also an important canonical problem, and it is noteworthy that CSM has been validated against DNS datasets of evaporating and non-evaporating droplet-laden flow in stationary turbulence in Pai & Subramaniam (2007). In that study CSM was shown to capture accurate trends of TKE and Lagrangian particle velocity autocorrelation with varying St_η as observed in DNS. We next review the DNS datasets used in this study, a summary of which is provided in table 1.

7.1. *Decaying turbulence: turbulence modification and dispersion statistics*

Sundaram & Collins (1999) have performed DNS of particle-laden freely decaying turbulence in the absence of gravity for several Stokes numbers. The system is volumetrically dilute, with particles in the sub-Kolmogorov size range, and collisions among particles, if any, are assumed to be elastic. Two-way coupling is assumed, i.e. the effect of the dispersed phase on fluid-phase momentum conservation is accounted for. Parameters of the homogeneous model problem are given in tables 2 and 3. In table 2, u' is the initial turbulence intensity in the fluid phase and v' is the initial turbulence intensity in the dispersed phase. These intensities are related to the respective TKE in each phase at initial time through $u'^2 = (2/3)k_f(0)$ and $v'^2 = (2/3)k_d(0)$. Initial conditions for the dispersed phase are given in table 3 and are taken from the DNS dataset at $T = 0.8$. This test case is hereafter referred to as SC.

Truesdell & Elghobashi (1994, hereafter TE) have performed DNS of particle dispersion in freely decaying turbulence with two-way coupling effects included. The dispersed-phase volume fraction is 2.5×10^{-4}, while the particle diameter scaled by the Kolmogorov length scale is 0.158. Initial conditions for the model comparison are taken from the DNS dataset at the time when the particles are introduced into the simulation. Parameters of the DNS dataset are given in table 4. TE report the evolution of the velocity autocorrelation of the dispersed phase, and that of the

Dispersed-phase volume fraction	α_d	1.8×10^{-4}
Fluid-phase thermodynamic density	ρ_f (kg m^{-3})	1.16
Dispersed-phase thermodynamic density	ρ_d (kg m^{-3})	1045.44
Kinematic viscosity of fluid	ν_f (m^2 s^{-1})	6.761×10^{-3}

TABLE 2. Unscaled parameters of the test case corresponding to particle-laden decaying turbulence used in this study – the DNS of Sundaram & Collins (1999) specifies the parameters to be in 'arbitrary' units, but we use SI units for this case. Acceleration due to gravity and initial mean slip between phases is zero for all cases.

$St_\eta = \tau_p/\tau_\eta$	u' (m s^{-1})	v' (m s^{-1})	ε_f (m^2 s^{-3})
1.6	0.802	0.773	0.363
3.2	0.794	0.738	0.403
6.4	0.793	0.744	0.438

TABLE 3. Particle–laden decaying turbulence test case (Sundaram & Collins 1999): initial values (unscaled) of the turbulence intensities u' and v' in the fluid phase and dispersed phase, respectively, and dissipation rate in the fluid phase, for different Stokes numbers.

St_η	ρ_d/ρ_f	ϕ
1.27	909	0.23
2.54	1818	0.45
5.09	3636	0.91

TABLE 4. Particle–laden decaying turbulence test case to investigate particle dispersion (Truesdell & Elghobashi 1994). For this test case, the following scaled parameter values are chosen: initial dissipation, $\varepsilon_f = 1.309 \times 10^{-3}$; initial TKE in both phases, $k_f = k_d = 2.85 \times 10^{-3}$; and kinematic viscosity, $\nu_f = 5.05 \times 10^{-5}$. In the DNS, all parameters are scaled by a reference length scale, $L_{ref} = 0.1859$ m, and a reference time scale, $T_{ref} = 0.11$ s.

gas-phase velocity 'seen' by the particles, which they refer to as the fluid velocity in the vicinity of the dispersed phase. This fluid velocity autocorrelation reported by TE is conditioned by the fact that it is measured along the trajectory of the dispersed particle. Since CSM is built on the concept of notional particles, proximity of the notional particles in physical space does not necessarily imply that a fluid particle and the dispersed particle are physically close to each other. Therefore, (4.17) provides an unconditioned estimate of the fluid–particle velocity autocorrelation, which is different from that reported by TE. We therefore do not compare this result with model predictions.

7.2. *Homogeneous shear: turbulence modification and dispersion statistics*

Ahmed & Elghobashi (2000) have performed two-way coupled DNS of homogeneously sheared turbulence laden with rigid particles (see figure 2). Of the several test cases analysed in that study, only the test cases involving varying mass

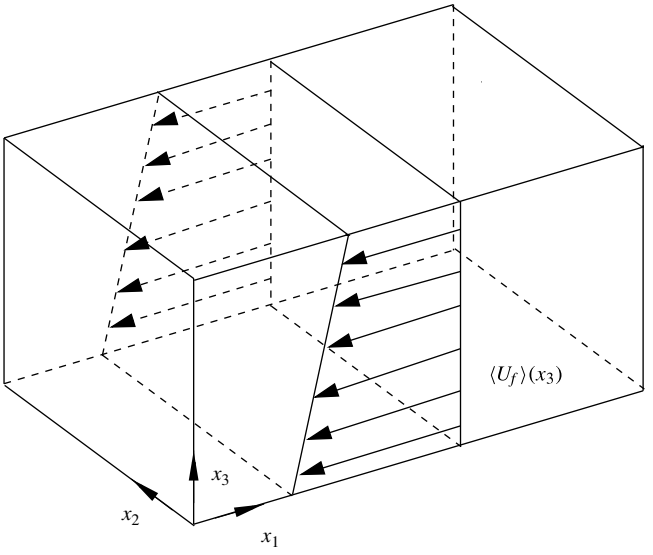

FIGURE 2. Schematic of the DNS of turbulent homogeneous shear laden with particles (Ahmed & Elghobashi 2000).

St_η	d	ρ_d/ρ_f	d/η	α_d
0.233 (C)	6.0×10^{-4}	525	0.0887	1.9×10^{-4}
0.583 (I)	1.0×10^{-3}	472.5	0.1479	2.1×10^{-4}
1.165 (H)	1.0×10^{-3}	945	0.1479	1.0×10^{-4}
2.33 (F)	1.0×10^{-3}	1890	0.1479	5.0×10^{-5}

TABLE 5. Scaled parameters for the particle-laden homogeneous shear test case: varying particle inertia (Ahmed & Elghobashi 2000) for a constant mass loading ratio $\phi = 0.1$. In the DNS, all parameters are scaled by a reference length scale, $L_{ref} = 0.39$ m, and reference time, $T_{ref} = 1$ s.

loading and varying particle inertia, in the absence of gravity, are considered here. A constant shear rate given by $\partial\langle U_1\rangle/\partial x_3 = \partial\langle V_1\rangle/\partial x_3 = \mathscr{S}$ is imposed on the fluid phase and the dispersed phases, respectively. The point particles are evolved according to the equation due to Maxey & Riley (1983), with an additional contribution arising from the mean shear. Parameters for the varying particle inertia test case are given in table 5. Parameters for the varying mass loading test case are given in table 6. This test case is hereafter referred to as AE-1.

Ahmed & Elghobashi (2001) have also performed solid particle dispersion studies in homogeneously sheared turbulence. The particle-laden system is dilute and one-way coupling is assumed. Parameters of the DNS dataset taken at the point of injection are presented in table 7. Simulations are performed for two shear numbers (shear number $= \mathscr{S} l/u_{rms}$), which in their DNS is the shear rate scaled by the large-eddy turnover time scale obtained from the eddy length scale l and the root mean square

ϕ	d	ρ_d/ρ_f	d/η	α_d
1 (B)	1.0×10^{-3}	1890	0.1479	5.0×10^{-4}
0.5 (G)	1.0×10^{-3}	1890	0.1479	2.5×10^{-4}
0.1 (F)	1.0×10^{-3}	1890	0.1479	5.0×10^{-5}

TABLE 6. Scaled parameters for the particle-laden homogeneous shear test case: varying mass loading (Ahmed & Elghobashi 2000) for a constant Stokes number $St_\eta = 2.33$. In the DNS, all parameters are scaled by a reference length scale, $L_{ref} = 0.39$ m, and reference time, $T_{ref} = 1$ s.

Shear number (Case)	d	St_η	ρ_d/ρ_f	d/η	α_d
2 (A)	1.02×10^{-4}	0.233	19000	0.0153	2.9938×10^{-9}
2 (B)	3.19×10^{-4}	2.33	19000	0.0477	9.0721×10^{-8}
4 (C)	7.25×10^{-5}	0.126	19000	0.0122	1.0626×10^{-9}

TABLE 7. Scaled parameters for the solid particle dispersion test case in homogeneous shear (Ahmed & Elghobashi 2001) for varying shear number in the absence of gravity. In the DNS, all parameters are scaled by a reference length scale, $L_{ref} = 1$ m, and reference time, $T_{ref} = 1$ s.

velocity u_{rms}. We compare CSM predictions of particle velocity autocorrelation with these DNS results. This test case is hereafter referred to as AE-2.

8. Model predictions

This section summarizes model predictions from CSM for the canonical test cases described earlier. Prior to assessing the predictions from CSM, we present the details of the integration of stochastic differential equations given by (4.1) and (4.2). Since in this study we are interested only in statistics of the two-phase flow, such as TKE and velocity autocorrelation, there are two approaches by which these statistics can be obtained from CSM. One approach (method 1) is to initialize a large number of *computational* particles according to a single-point velocity distribution with a prescribed Reynolds stress tensor, if required, and integrate their velocities in time according to the system of SDEs (4.1) and (4.2). Since we focus on homogeneous systems in this study, there is no need to track particle positions in time. A numerical scheme suitable for such systems, for example an Euler–Maruyama scheme (Kloeden & Platen 1992), can be employed, and the implied TKE and velocity autocorrelation can be computed from the computational ensemble. The second approach (method 2) is to integrate the *ordinary* differential equations (ODEs) given by (4.7) and (4.8) for the evolution of the Reynolds stresses and by (4.17) and (4.18) for the evolution of the velocity autocorrelation in time. From the Reynolds stresses for each phase, the TKE in each phase can be obtained by computing half the trace of the Reynolds stress tensor. At the end of each ODE time step, the time scales (τ_1, τ_2, τ_3, τ_4 and τ) are recomputed from the statistics obtained at the penultimate step. Since none of the statistics or time scales depend on the fluctuating velocities $\boldsymbol{u}$ and $\boldsymbol{v}$, this second method is very useful for our study. Another reason that makes this second approach attractive is that, since we are integrating only the ODEs, there is zero statistical error and there is no need to track a large number of computational particles in time. Note, however, that this latter method is legitimate only for the homogeneous system

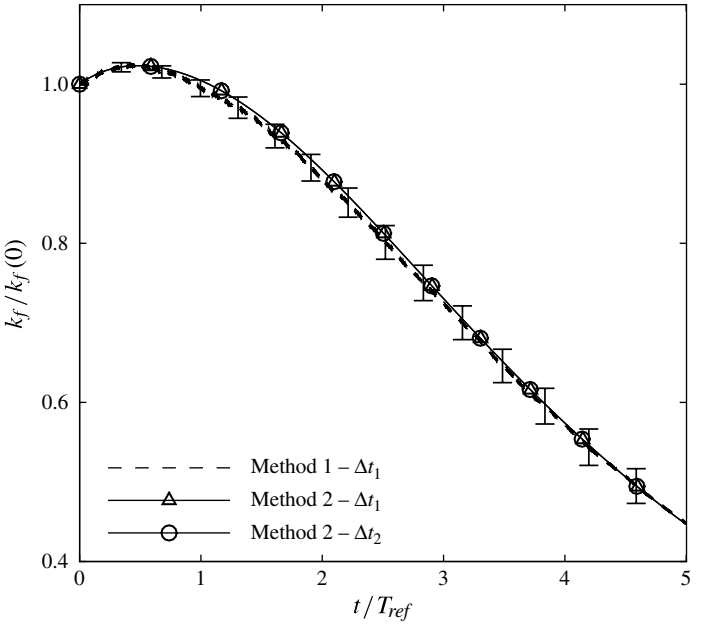

FIGURE 3. Comparison between method 1 shown with dashed lines (integration of SDEs given by (4.1) and (4.2) and computing the TKE from the computational ensemble) and method 2 shown with solid lines (integrating the ODEs given by (4.7) and (4.8)) and computing the trace of the Reynolds stress tensor for case B of particle-laden homogeneous shear from AE-1. Two time steps Δt_1 and Δt_2 are employed for method 2 to illustrate convergence with the Euler time stepping. Also shown are 95 % confidence intervals corresponding to method 1 obtained by averaging over 20 multiple independent simulations.

employed in this study; inhomogeneity will dictate that the computational particle positions and velocities be evolved in time.

A comparison between methods 1 and 2 for case B of particle-laden homogeneous shear is presented in figure 3. For method 1, the Euler–Maruyama scheme is employed to track an ensemble of 10 000 computational particles and statistics are averaged over 20 multiple independent simulations. The time step size chosen is $\Delta t_1 = 0.0005 \min(\tau_p, \tau)$. For method 2, an explicit Euler time stepping scheme is employed, with two time step sizes Δt_1 and $\Delta t_2 = 0.002 \min(\tau_p, \tau)$. Figure 3 illustrates that the results obtained from the Euler time stepping of the ODEs is almost indistinguishable for the time steps chosen, thereby illustrating convergence of the integration scheme with respect to time step. Results obtained from the Euler–Maruyama scheme for the integration of the SDEs are close to those obtained by method 2. Since it is computationally less expensive to integrate the ODEs in time, we adopt method 2, with a time step size equal to Δt_2, to obtain the evolution of the statistics for all cases in the rest of this study.

8.1. *Case I*

8.1.1. *Prediction of TKE in particle-laden decaying turbulence*

For the case of homogeneous decaying turbulence in the absence of mean velocity gradients, the implied evolution equations for the TKE in the fluid phase and dispersed

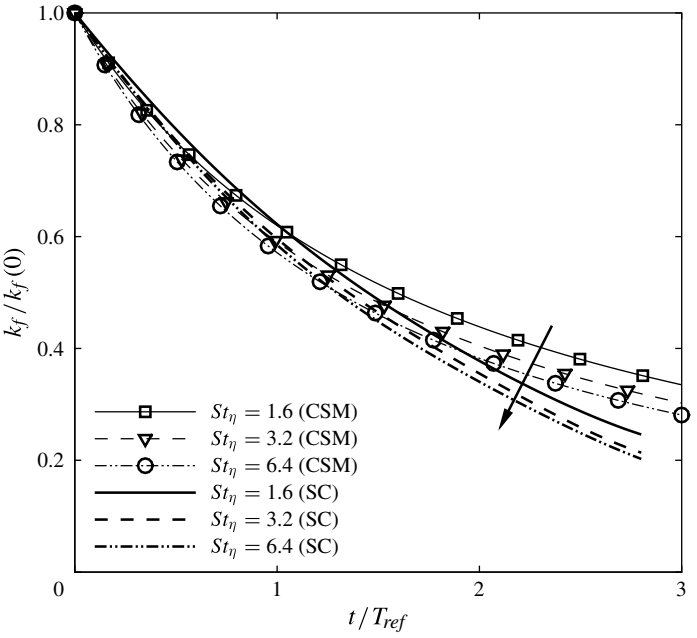

FIGURE 4. Evolution of TKE in the fluid phase for varying Stokes number in particle-laden homogeneous decaying turbulence (Case I), alongside results from DNS (Sundaram & Collins 1999). The arrow indicates the direction of increasing Stokes number.

phases are given by (4.13) and (4.14), respectively. The only two terms that govern the evolution of the TKE in the fluid phase are the interphase TKE transfer term Π_{k_f} and the fluid-phase dissipation ε_f.

Figure 4 shows the predicted evolution of the fluid-phase TKE by CSM for varying initial Stokes numbers St_η. Shown alongside are corresponding results from DNS data SC. For a system with sub-Kolmogorov particles with no production due to particle wakes, the higher the particle inertia, faster is the decay of energy in the carrier and dispersed phases. This implies that the time scale of decay of TKE *decreases* with increasing Stokes number. Increasing particle inertia results in an increased interphase TKE transfer (as the fluid phase has to do more work in dispersing the particles). However, the increased dissipation due to the presence of the particles and bulk viscous dissipation offsets the increased interphase TKE, thereby leading to a faster decay in fluid-phase TKE. This behaviour is clearly seen in the DNS results. CSM accurately reproduces the trend of TKE evolution observed in DNS for varying Stokes number. Since the interphase TKE is equal and opposite in the dispersed phase, the evolution of dispersed-phase TKE also depicts an identical trend as in the fluid phase. The evolution of the dispersed-phase TKE is shown in figure 5 alongside DNS results, which again illustrates that CSM accurately captures the trend of TKE decay with increasing Stokes number. The reason why CSM successfully captures this trend correctly is due to the use of the multiscale interaction time scale $\langle \tau_{int} \rangle$ as the time scale for interphase TKE transfer. As noted earlier, drag models based on the particle response time scale fail to capture this trend of TKE decay with increasing Stokes number (Pai & Subramaniam 2006).

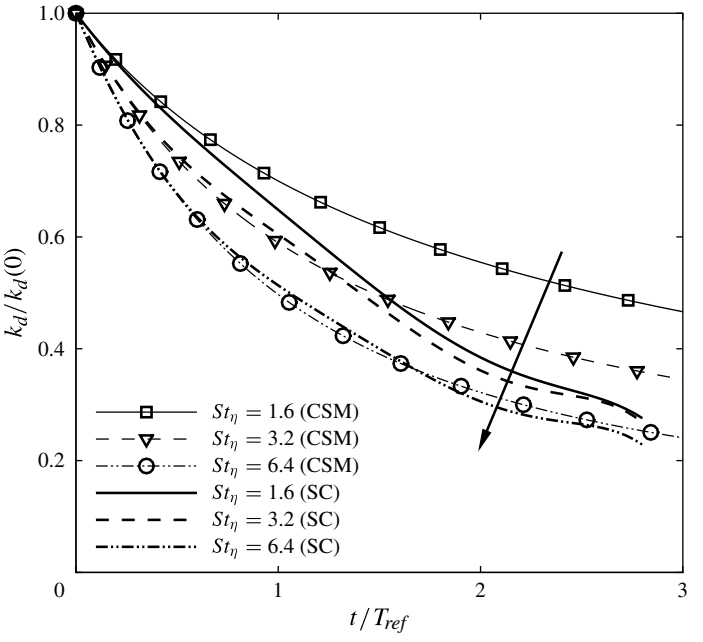

FIGURE 5. Evolution of TKE in the dispersed phase for varying Stokes number in particle-laden homogeneous decaying turbulence (Case I), alongside results from DNS (Sundaram & Collins 1999). The arrow indicates the direction of increasing Stokes number.

8.1.2. *Prediction of particle velocity autocorrelation in particle-laden decaying turbulence*

Figure 6 shows the predicted evolution of the particle velocity autocorrelation in decaying turbulence given by (4.16) for a range of Stokes numbers for the test case TE. Also shown on the same plot are corresponding results from DNS (Truesdell & Elghobashi 1994). With increasing particle Stokes number, the decay in particle velocity autocorrelation is slower, since particles with larger inertia lose correlation with their earlier velocities more slowly. This implies that the time scale of decay of particle velocity autocorrelation *increases* with increasing Stokes number. CSM accurately captures this trend of decay of particle velocity autocorrelation with varying Stokes numbers, although CSM is less sensitive to Stokes number for increasing particle inertia. Interestingly, the particle velocity autocorrelation behaves in an identical manner in stationary turbulence (Pai & Subramaniam 2007), where CSM is again successful in reproducing trends observed in DNS. Since the rate at which a particle loses correlation with its earlier velocity is primarily determined by its inertia, the behaviour of a heavy particle is essentially the same in decaying and stationary turbulence.

It is noteworthy to recapitulate at this point that two-phase turbulence models in which the interphase TKE transfer evolves on the particle response time scale τ_p (see Pai & Subramaniam 2006) do not possess the capability to capture *simultaneously* the decay trend in the TKE and the decay trend in particle velocity autocorrelation with varying Stokes number. Models employed in LE statistical implementations of two-phase flows fall in this category (see e.g. Amsden *et al.* 1989).

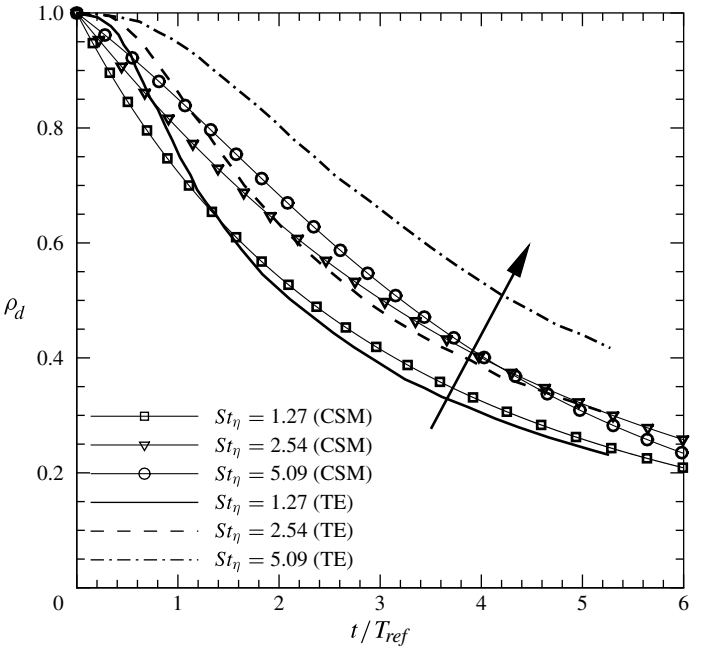

FIGURE 6. Evolution of dispersed-phase velocity autocorrelation for varying Stokes number in particle-laden decaying turbulence (Case I), alongside results from DNS (Truesdell & Elghobashi 1994). The arrow indicates the direction of increasing Stokes number.

8.2. *Case II*

8.2.1. *Prediction of TKE in particle-laden homogeneous shear*

For a uniform mean shear (say in the 1–3 direction as $\partial\langle U_i\rangle/x_j = \partial\langle V_i\rangle/x_j = \mathscr{S}\delta_{i1}\delta_{j3}$), the implied evolution equations for the Reynolds stresses are (4.7) and (4.8), and those for the TKE are (4.9) and (4.10). The evolution equation for the dissipation rate ε_f is given by (5.7), which includes the effect of mean velocity gradient. The computations are initialized at time $\mathscr{S}t = 1$ when the carrier-phase turbulence in the DNS (Ahmed & Elghobashi 2000) is fully developed. At this time, the stochastic particles that represent the fluid and the dispersed phases are initialized with zero mean and covariance given by $\langle u_i u_j\rangle = 2k_f[b_{ij} + (1/3)\delta_{ij}]$ and $\langle v_i v_j\rangle = 2k_d[b_{ij} + (1/3)\delta_{ij}]$, respectively. The components of the initial anisotropy tensor b_{ij}, which is the same for both the phases, are $b_{11} = 3.62 \times 10^{-2}$, $b_{22} = -4.41 \times 10^{-2}$, $b_{33} = 0.79 \times 10^{-2}$ and $b_{13} = b_{31} = -1.22 \times 10^{-1}$ at $\mathscr{S}t = 1$. The scaled fluid-phase dissipation ε_f at this scaled time is 5.77×10^{-4}, and the scaled fluid kinematic viscosity ν_f is 1.05×10^{-4}. The test cases investigated in this study are denoted B, G, F, C, I, H and F (identical to that in the DNS) and parameters corresponding to these test cases are given in tables 6 and 7 (see table captions for the reference length and time scales employed to scale all dimensional parameters).

Figure 7 shows the predicted evolution of the fluid-phase TKE by CSM for varying Stokes numbers (particle inertia) and constant mass loading of $\phi = 0.1$. These test cases correspond to cases C, I, H and F in the DNS AE-1. It is difficult to predict the evolution of the TKE based on simple physical arguments as was possible in Case I for particle-laden homogeneous decaying turbulence. This is primarily because there are competing effects of fluid-phase dissipation and production due to the mean

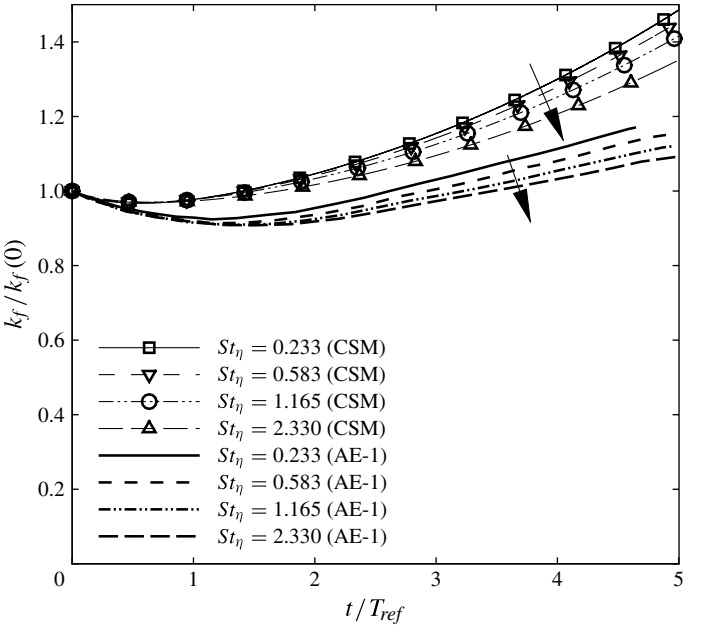

FIGURE 7. Evolution of fluid-phase TKE for varying particle inertia and constant mass loading $\phi = 0.1$ (Case II), alongside results from DNS (Ahmed & Elghobashi 2000). The arrows indicate the direction of increasing particle inertia.

shear coupled with the interphase TKE transfer. Relative magnitudes of these terms are difficult to estimate based on scaling arguments in this case. Figure 7 shows that the DNS predicts a fluid-phase TKE that increases at a slower rate for increasing particle inertia (or Stokes number) at constant mass loading, a trend that is accurately captured by CSM. Interestingly, this trend with increasing particle inertia is identical to that observed in Case I for homogeneous decaying turbulence. As shown in Xu & Subramaniam (2006), EE models for interphase TKE transfer based on the particle response time scale τ_p are incapable of capturing this trend.

Figure 8 shows the predicted evolution of the fluid-phase TKE by CSM for varying mass loading and constant particle response time $\tau_p = 1.0$. These test cases correspond to the cases B, G and F in the DNS AE-1. For increasing mass loading, the DNS shows a slower rate of increase in k_f. CSM predicts the trends accurately after scaled time $t/T_{ref} = 1.2$, but predicts a cross-over at initial time. Close inspection of the DNS results (see figure 46 in Ahmed & Elghobashi (2000)) in fact reveals a similar cross-over, although not as conspicuous as predicted by CSM.

8.2.2. *Prediction of particle velocity autocorrelation in particle-laden homogeneous shear*

The evolution for velocity autocovariance in the fluid phase in the presence of a constant mean shear as implied by CSM is given by (4.17), while that for the dispersed phase is given by (4.18). Note that, just as in SLM for single-phase homogeneous shear flows (Pope 2002), the autocovariance tensor is not symmetric. This is due to an additional mean shear term in the evolution of $\langle u_3(t_0)u_1(t)\rangle$ that does not appear in the evolution of the $\langle u_1(t_0)u_3(t)\rangle$ component.

Figure 9 shows the results from the DNS of AE-2. Cases A and C have the same particle response time $\tau_p = 0.236$, but different shear numbers. The DNS results show

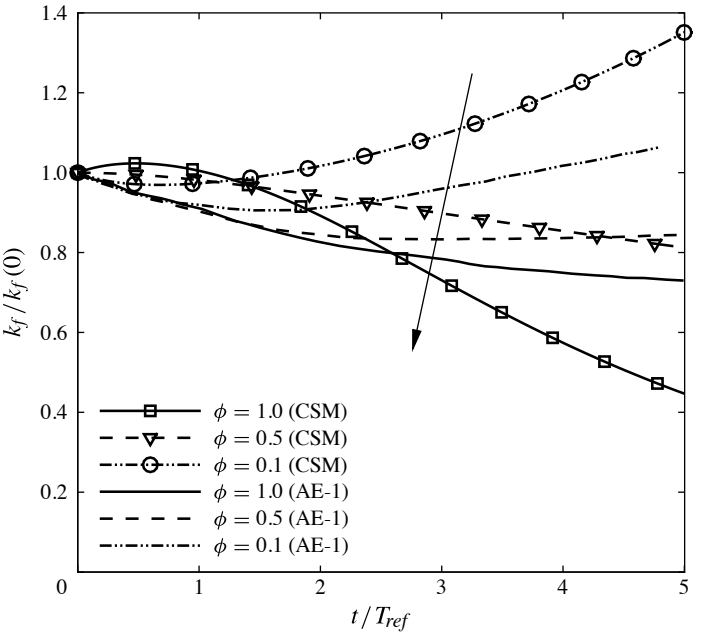

FIGURE 8. Evolution of fluid-phase TKE for varying mass loading and constant particle inertia $\tau_p = 1.0$ (Case II), alongside results from DNS (Ahmed & Elghobashi 2000). The arrow indicates the direction of increasing mass loading.

that the dispersed particles retain a stronger correlation with their earlier velocities for a shear number equal to 4 than for a shear number equal to 2 (see figure 9*a*). The same behaviour is observed in the DNS for the fluid points as well. As explained in Ahmed & Elghobashi (2001), the reason for the higher velocity autocorrelation for case C compared to case A is that the gas-phase turbulent kinetic energy in case C is less than that in case A. Consequently, the ability of the gas-phase fluctuating velocity to disperse the particles is smaller for case C than for case A, thereby leading to a higher velocity autocorrelation in case C. Predictions from CSM for the dispersed-phase and fluid-phase velocity autocorrelation ρ_{11} for cases A and C are shown in figure 9(*b*). CSM is able to capture the trend with increasing shear number for both the fluid-phase and dispersed-phase velocity autocorrelation, as indicated by the direction of the arrow in the figure.

The DNS predicts that, for the particle response time scale employed for the cases A and C, the dispersed-phase velocity autocorrelation and the fluid-phase velocity autocorrelation match (more so for case C). It appears that the DNS results predict a match of fluid-phase and dispersed-phase velocity autocorrelations for Stokes numbers $0 < St_\eta \ll 1$. This behaviour is not quantitatively captured by CSM, although the trend with increasing shear number is captured accurately. The reason why the predictions for the dispersed-phase and fluid-phase velocity correlation from CSM do not match exactly can be explained by noting that the time scales for the evolution of the dispersed-phase and fluid-phase velocity autocorrelation are identical only in the limit $St_\eta \to 0$ (see (6.4) and (6.2) and the subsequent discussion), which is the physically correct limit at which the dispersed particles behave as fluid tracers.

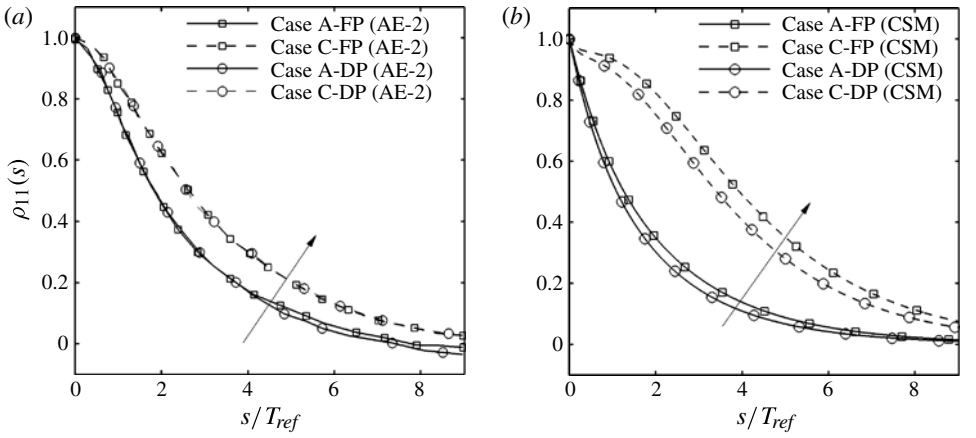

FIGURE 9. Predicted evolution of velocity autocorrelation in fluid phase (FP) and dispersed phase (DP) corresponding to cases A and C for particle-laden homogeneous shear turbulence: (*a*) DNS results (Ahmed & Elghobashi 2001); and (*b*) CSM predictions. The arrows indicate the direction of increasing shear number.

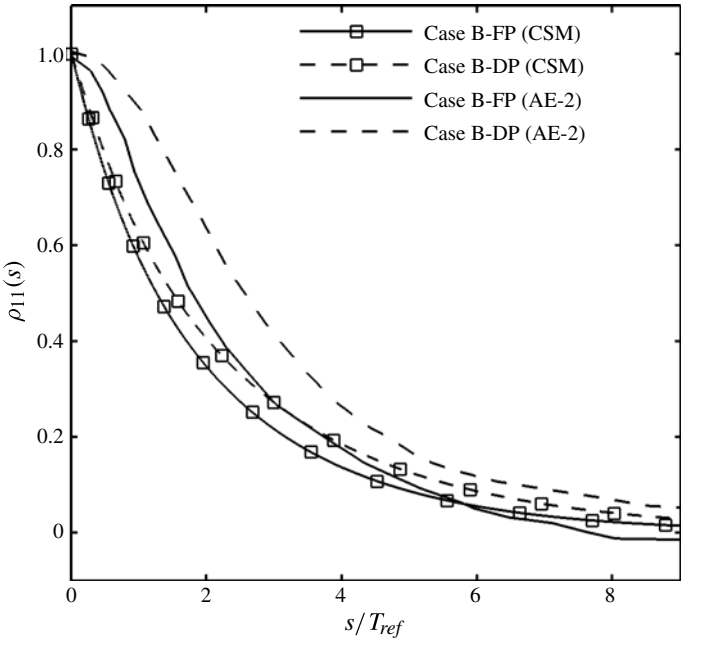

FIGURE 10. Predicted evolution of velocity autocorrelation of fluid phase (FP) and dispersed phase (DP) from CSM corresponding to case B for particle-laden homogeneous shear turbulence. Results from DNS (Ahmed & Elghobashi 2001) are shown alongside.

In figure 10, dispersed-phase and fluid-phase velocity autocorrelations are shown for the case with higher particle inertia (case B). In this case, the DNS predicts that the two velocity autocorrelations are not identical to each other; CSM captures this behaviour for this case. The observation from the DNS that the dispersed-phase

velocity autocorrelation is slightly higher than the fluid-phase velocity autocorrelation due to particle inertia is also captured by CSM.

Ahmed & Elghobashi (2001) have also performed particle dispersion studies in the presence of particle drift. They note that the velocity autocorrelation in the 2 direction is affected by the particles crossing oblique vortices as they traverse in the direction of gravity. Also, they observe that the particle velocity autocorrelation exhibits negative loops to account for the continuity effect (Csanady 1963) in the presence of particle drift.

The ability of two-phase flow models to capture the negative loops in the particle velocity autocorrelation, in the presence of particle drift, has received widespread interest. Gouesbet, Berlemont & Picart (1984) derive an expression that relates the spectral tensor corresponding to the Lagrangian particle velocity to that corresponding to the fluid-phase velocity autocorrelation. They use a Frenkiel form for the fluid-phase velocity autocorrelation and, under further simplifications (absence of Basset forces), show the presence of negative loops in the particle velocity autocorrelation. Mei, Adrian & Hanratty (1991) employ a Fourier representation of the particle equation of motion for small Reynolds number and large density ratio (Maxey & Riley 1983) and, under assumptions of Gaussian particle velocity field, Corrsin's conjecture (Corrsin 1959) and an isotropic turbulent velocity field, analytically derive a set of integral equations for calculating the autocorrelation of fluid-phase velocity at the location of the dispersed particles. They further calculate the particle diffusivities from the knowledge of the fluid-phase velocity autocorrelation at the location of the particle. With increasing drift velocity, they show that the fluid-phase velocity autocorrelation exhibits negative loops that account for the rapid particle motion from a region of positive (or negative) velocity into a region of negative (or positive) velocity.

In the foregoing studies, the capability of capturing continuity effects is built in to the dispersed-phase velocity autocorrelation. Lagrangian particle-based methods such as the one explored in this work do not directly solve for the velocity autocorrelation. On the other hand, an evolution equation for the particle velocity (cf. (4.1) and (4.2)) implies an evolution of the Lagrangian velocity autocorrelation. Thus the capability of capturing continuity effects in Lagrangian particle-based methods needs to be built in to the particle evolution equations. Several studies have been devoted to employing two-phase models based on the Langevin equation for particle dispersion. Pozorski & Minier (1999) use Csanady's expressions for the Lagrangian integral time scale of the fluid along and transverse to the gravity directions in their Langevin equation to capture the crossing trajectories effect, while Pascal & Oesterlé (2000) propose a model for the drift term that incorporates an exponentially decaying velocity autocorrelation. Such models that are based on the Langevin equation do not possess the capability to capture the manifestation of the continuity effect in the velocity autocorrelation, since the velocity autocorrelation can never become negative when such models are employed (the evolution of the velocity autocovariance based on a Langevin equation is essentially exponential with no negative loops). Since CSM is also based on the Langevin equation, the evolution of velocity autocorrelation is exponential with no negative loops as well (cf. (4.17) and (4.18)) and hence the model does not currently possess the capability to capture crossing trajectory effects.

9. Discussion

Turbulent particle-laden flows are characterized by the presence of a multitude of time and length scales. The capability of a two-phase flow model to capture the

time scales associated with interphase turbulent kinetic energy transfer and inertial particle dispersion in canonical particle-laden turbulent flows determines its predictive capability in more complex flows. We now assess the new model by summarizing its principal features that make it suitable to model two-phase flows, and also its behaviour in limiting cases.

(*a*) The formulation of CSM, and the EoE concept, together contain important non-dimensional quantities that can be derived purely based on a dimensional analysis of a two-phase flow, which are St_η, mass loading ϕ and volume fraction α_d. Although it is desirable that a two-phase flow model be a function of these non-dimensional quantities, it is clearly not sufficient, as there are time and length scales corresponding to important interphase processes encountered in two-phase flows that a two-phase model must be able to capture.

(*b*) CSM possesses the capability of capturing the disparate time scale trends of TKE and velocity autocorrelation decay with St_η that are observed in DNS of particle-laden turbulence. This is achieved through the multiscale interaction time scale $\langle\tau_{int}\rangle$, and the form of the drift and diffusion terms.

(*c*) CSM has the correct limiting behaviour as $St_\eta \to 0$ and $\phi \to 0$ (see discussion in § 6.2).

(*d*) In order to assess the behaviour of CSM in the limit $St_\eta \to \infty$ at constant mass loading, we consider for the sake of simplicity the case with no production due to mean shear.

(i) *Effect of large St_η on k_d.* In the limit $St_\eta \to \infty$, we expect the dispersed phase to remain unaffected by the presence of the fluid phase due the large inertia in the former. Such a two-phase flow is characterized by a highly collisional dispersed phase much like a granular flow. In such a flow with elastic collisions and in the absence of any form of dissipation in the dispersed phase, the dispersed-phase TKE should remain constant in time.

Consider (6.1) in the limit of large Stokes number. As $St_\eta \to \infty$, the EoE constant $C_k \to 0$, which implies that $\rho_d\alpha_d k_d^e \to 0$. Then τ_4 is essentially equal to τ_p (see discussion in § 6.3). However, $St_\eta \to \infty$ also implies that $\tau_p \to \infty$, which in turn implies that $\mathrm{d}k_d/\mathrm{d}t \to 0$ (cf. (4.12)). Thus in the limit $St_\eta \to \infty$ at constant mass loading and for elastically colliding dispersed-phase elements, CSM predicts that the dispersed-phase TKE does not evolve (or decays very slowly) in time.

(ii) *Effect of large St_η on k_f.* Since $C_k \to 0$, the specific TKE energy in the fluid phase $\rho_f\alpha_f k_f \to \rho_m k_m$ (cf. (5.4)). From (4.13) and using the relation $\rho_m k_m = \rho_f\alpha_f k_f + \rho_d\alpha_d k_d$, one may write

$$\frac{\mathrm{d}}{\mathrm{d}t}(\rho_f\alpha_f k_f) \sim -\frac{\rho_d\alpha_d k_d}{\tau_p} - \rho_f\alpha_f\varepsilon_f = -\rho_f\alpha_f\varepsilon_f, \tag{9.1}$$

where the fact that k_d remains constant and $\tau_p \to \infty$ has been employed. Interestingly, CSM predicts that the TKE in the fluid phase decays much like in a single-phase flow; if the dissipation rate ε_f is a constant, then a linear decay of k_f is predicted in the fluid phase.

(iii) *Effect of large St_η on τ_3.* As $St_\eta \to \infty$, one can show that $1/\tau_3 \to C_1\phi/(\tau C_3)$ (cf. (6.2)). This implies that the dispersed-phase velocity autocorrelation given by (4.20) decays exponentially, provided the time scale τ remains a constant. An exponential decay of velocity autocorrelation is also observed in elastic

hard-sphere event-driven molecular dynamics (MD) simulations (Alder & Wainwright 1970). Clearly, one cannot expect the $t^{-3/2}$ decay observed in these MD simulations at long time from the Langevin equation that is used as a basis of CSM.

(iv) *Effect of large St_η on τ_1.* As $St_\eta \to \infty$, one may expect that $1/(2\tau_1) \gg [1/2 + (3/4)C_0]1/\tau$ (cf. $A(t)$ in (4.2)). Thus from (4.19), CSM predicts an exponential decay for the fluid-phase velocity autocorrelation in the limit $St_\eta \to \infty$ as well. It remains to be verified from DNS of high-Stokes-number particle-laden flows if this is indeed true.

(*e*) In order to assess the behaviour of CSM in the limit $\phi \to \infty$ at constant St_η, we again consider the case with no production due to mean shear.

(i) *Effect of large ϕ on k_d.* In the limit $\phi \to \infty$, the EoE concept predicts that $C_k \to 1$ (cf. (6.1)). This implies that $\rho_d \alpha_d k_d^e \to \rho_m k_m$ and $\rho_f \alpha_f k_f^e \to 0$. It is easy to show then that

$$\frac{\mathrm{d}(\alpha_d \rho_d k_d)}{\mathrm{d}t} = \frac{\rho_f \alpha_f k_f}{\tau_\pi}. \tag{9.2}$$

For a constant St_η, the multiscale interaction time scale τ_π is a constant. Dividing both sides of (9.2) by $\rho_d \alpha_d$ (both ρ_d and α_d are constant for the homogeneous particle-laden turbulent flow in this study, and $\alpha_d \neq 0$), and observing that in the limit $\phi \to \infty$, the right-hand side approaches zero, one may conclude that CSM predicts k_d to be a constant in this limit. Interestingly, this behaviour of k_d is identical to that predicted in the limit $St_\eta \to \infty$.

(ii) *Effect of large ϕ on k_f.* It is easy to show also in the limit $\phi \to \infty$ that

$$\frac{\mathrm{d}(\alpha_f \rho_f k_f)}{\mathrm{d}t} = -\frac{\rho_f \alpha_f k_f}{\tau_\pi} - \rho_f \alpha_f \varepsilon_f. \tag{9.3}$$

In this strongly two-way coupled limit, the decay of fluid-phase TKE is due to two sources, as observed from (9.3): one due to the interphase TKE transfer k_f/τ_π (note that k_f/τ_π is positive) and the other due the dissipation ε_f. For a constant ε_f, k_f decays exponentially to zero over the time scale τ_π. A physical problem in this limit is a nearly close-packed particle-laden flow in which the carrier phase does work in making its way through the interstices between particles, and thus loses energy at a higher rate compared to the case with lower mass loading.

(iii) *Effect of large ϕ on τ_3.* As $\phi \to \infty$, the time scale $1/\tau_1 \to \infty$. In this limit, one may expect that the most significant contribution to $1/\tau_3$ is from $1/\tau_1$ (since $1/\tau_1$ appears in (6.2)). This implies that the dispersed-phase velocity autocorrelation given by (4.20) decays exponentially over a time scale $\tau_3 \to 0$.

(iv) *Effect of large ϕ on τ_1.* The same observation holds for (4.19) where $1/\tau_1 \to \infty$ and an exponential decay of the fluid-phase velocity autocorrelation is observed. It remains to be verified from DNS with high mass loading if this behaviour of the fluid-phase and dispersed-phase velocity autocorrelation is indeed true.

It is remarkable that the new CSM, coupled with the EoE concept, possesses several desirable limiting behaviours of two-phase flow models. However, additional datasets from DNS of two-phase flows in the limit $St_\eta \to \infty$ and $\phi \to \infty$ are needed to confirm the behaviour of CSM in these limits.

10. Conclusion

The ability of a two-phase flow model to capture the correct interphase transfer of turbulent kinetic energy and particle dispersion characteristics in a two-way coupled particle-laden flow is important for engineering applications but is a challenging modelling problem. Furthermore, DNS datasets show that these processes evolve on different time scales that have a disparate behaviour with Stokes number. With this perspective, the principal conclusions and achievements of this study are summarized below.

(*a*) Combining multiscale modelling ideas from the equilibration of energy concept, we have proposed a new coupled stochastic model that possesses the unique capability of capturing the disparate time scales corresponding to interphase TKE transfer and velocity autocorrelation, in addition to the behaviour of these time scales with varying Stokes numbers and mass loading.

(*b*) CSM is shown to possess the correct behaviour in the limit $St_\eta \to 0$ and $\phi \to 0$. CSM is therefore an excellent candidate to be employed for a particle-laden flow, such as in a coal gasifier that contains regions of high mass loading and regions of low mass loading in the same two-phase flow.

(*c*) CSM is tested in a range of homogeneous particle-laden flows, from two-way coupled particle-laden decaying turbulence and homogeneous shear to one-way coupled particle dispersion. CSM is shown to capture the evolution trends of important two-phase flow statistics such as TKE, velocity autocorrelation and fluid-phase dissipation for varying Stokes number and mass loading in all the two-phase flows studied in this work. Such a level of versatility of a two-phase flow model, especially the ability to capture simultaneously the correct trends of TKE decay with Stokes number in particle-laden *decaying* turbulence and the dependence of the stationary TKE on Stokes number in statistically *stationary* turbulence (see Pai & Subramaniam 2007, for more details) has not been demonstrated in the literature.

(*d*) CSM possesses several of the desirable limiting behaviours of two-phase flow models. In the limit $St_\eta \to \infty$ and $\phi \to \infty$, although the predicted behaviour of CSM appears reasonable, it would still need to be ascertained by performing DNS of particle-laden turbulent flows in this limit.

It will be interesting to assess the behaviour of CSM in inhomogeneous flows such as particle-laden jets, channel flows and mixing layers. For this, CSM will need to be extended to incorporate effects of mean pressure gradient and arbitrary mean velocity gradients into its formulation.

Acknowledgements

This work is partially supported by a US Department of Energy, Early Career Principal Investigator Program Grant No. DE-FG02-03ER25550.

Appendix. Particle method solution of the p.d.f. evolution equation

In this section, we review a popular particle method solution to the two-phase phasic p.d.f. transport equation (2.7). An ensemble of N_f notional particles represents the fluid phase, while an ensemble of N_p notional particles represents the dispersed phase. The ith notional particle is assigned a statistical weight $W^f_{(i)}$ corresponding to the fluid phase, and $W^p_{(j)}$ corresponding to the dispersed phase. The statistical weights satisfy the

following constraints:

$$\langle N_p \rangle = \sum_{j=1}^{N_p} W^p_{(j)}, \tag{A 1}$$

$$\alpha^*_d = \frac{v_d}{V} \sum_{j=1}^{N_p} W^p_{(j)} = \frac{v_d}{V} \langle N_p \rangle, \tag{A 2}$$

$$\alpha^*_f = 1 - \frac{v_d}{V} \sum_{j=1}^{N_p} W^p_{(j)} = \sum_{i=1}^{N_f} W^f_{(i)}, \tag{A 3}$$

where $\langle N_p \rangle$ is the mean number of real (physical) particles in the cell or measurement volume, v_d is the mean volume per dispersed particle, and V is the cell or measurement volume. The modelled volume fractions α_f and α_d are shown with asterisks. Together, the statistical weight $W^f_{(i)}$ and the p.d.f. $f^*_{\boldsymbol{U}}$, and $W^p_{(j)}$ and the p.d.f. f^*_V, model the evolution of $\alpha_\beta f_{\boldsymbol{U}|I_\beta}$ (for $\beta = \{f, d\}$) given by (2.7). In practice, the FP equations (3.3) and (3.4) are not solved directly, but the SDEs given by the system in (3.2) are advanced in time using computational particles. The time evolution of these particles indirectly solves the FP equation. The above implementation for notional particles and statistical weights corresponds to a computational ensemble with equal statistical weights assigned to each notional particle. Since we focus on homogeneous flows in this study, we assume equal statistical weights corresponding to each notional particle and therefore do not track the weights in time. One can also conceive of an implementation where the statistical weight associated with each notional particle evolves in time as is done in Garg, Narayanan & Subramaniam (2009) for inhomogeneous two-phase flows.

REFERENCES

AHMED, A. M. & ELGHOBASHI, S. 2000 On the mechanisms of modifying the structure of turbulent homogeneous shear flows by dispersed particles. *Phys. Fluids* **12** (11), 2906–2930.

AHMED, A. M. & ELGHOBASHI, S. 2001 Direct numerical simulation of particle dispersion in homogeneous turbulent shear flows. *Phys. Fluids* **13** (11), 3346–3364.

ALDER, B. J. & WAINWRIGHT, T. E. 1970 Decay of the velocity autocorrelation function. *Phys. Rev.* A **1** (1), 18–21.

AMSDEN, A. A., O'ROURKE, P. J. & BUTLER, T. D. 1989 KIVA-II: a computer program for chemically reactive flows with sprays. *Tech. Rep.* LA-11560-MS. Los Alamos National Laboratory.

BOIVIN, M., SIMONIN, O. & SQUIRES, K. 1998 Direct numerical simulation of turbulence modulation by particles in isotropic turbulence. *J. Fluid Mech.* **375**, 235–263.

CHAGRAS, V., OESTERLE, B. & BOULET, P. 2005 On the heat transfer in gas–solid pipe flows: effects of collision induced alterations of the flow dynamics. *Intl J. Heat Mass Transfer* **48**, 1649–1661.

CHEN, X.-Q. & PEREIRA, J. C. F. 1997 Efficient computation of particle dispersion in turbulent flows with a stochastic–probabilistic model. *Intl J. Heat Mass Transfer* **40** (8), 1727–1741.

CORRSIN, S. 1959 Progress report on some turbulent diffusion research. *Adv. Geophys.* **6**, 161–164.

CSANADY, G. T. 1963 Turbulent diffusion of heavy particles in the atmosphere. *J. Atmos. Sci.* **20**, 201–208.

FADLUN, E. A., VERZICCO, R., ORLANDI, P. & MOHD-YUSOF, J. 2000 Combined immersed-boundary finite-difference methods for three-dimensional complex flow simulations. *J. Comput. Phys.* **161** (1), 35–60.

GAO, Z. & MASHAYEK, F. 2004 Stochastic modeling of evaporating droplets polydispersed in turbulent flows. *Intl J. Heat Mass Transfer* **47**, 4339–4348.

GARDINER, C. W. 1983 *Handbook of Stochastic Methods*. Springer.

GARG, R., NARAYANAN, C. & SUBRAMANIAM, S. 2009 A numerically convergent Lagrangian–Eulerian simulation method for dispersed two-phase flows. *Intl J. Multiphase Flow* **35** (4), 376–388.

GOSMAN, A. D. & IOANNIDES, E. 1983 Aspects of computer simulation of liquid fueled combustors. *J. Engine Res.* **6** (7), 482–490.

GOUESBET, G., BERLEMONT, A. & PICART, A. 1984 Dispersion of discrete particles by continuous turbulent motions. Extensive discussion of the Tchen's theory, using a two-parameter family of Lagrangian correlation functions. *Phys. Fluids* **27** (4), 827–837.

GROSZMANN, D. E. & ROGERS, C. B. 2004 Turbulent scales of dilute particle-laden flows in microgravity. *Phys. Fluids* **16** (12), 4671–4684.

HAWORTH, D. C. & POPE, S. B. 1986 A generalized Langevin model for turbulent flows. *Phys. Fluids* **29**, 387–405.

HU, H., ZHU, M. Y. & PATANKAR, N. A. 2001 Direct numerical simulations of fluid–solid systems using the arbitrary Lagrangian–Eulerian technique. *J. Comput. Phys.* **169** (2), 427–462.

KLOEDEN, P. & PLATEN, E. 1992 *Numerical Solution of Stochastic Differential Equations*. Springer.

LU, Q. Q. 1995 An approach to modeling particle motion in turbulent flows – I. Homogeneous, isotropic turbulence. *Atmos. Environ.* **29** (3), 423–436.

L'VOV, V. S., OOMS, G. & POMYALOV, A. 2003 Effect of particle inertia on turbulence in a suspension. *Phys. Rev.* E **67**, 046314.

MASHAYEK, F. 1999 Stochastic simulations of particle-laden isotropic turbulent flow. *Intl J. Multiphase Flow* **25**, 1575–1599.

MASHAYEK, F., JABERI, F. A., MILLER, R. S. & GIVI, P. 1997 Dispersion and polydispersity of droplets in stationary isotropic turbulence. *Intl J. Multiphase Flow* **23**, 337–355.

MAXEY, M. R. & RILEY, J. J. 1983 Equation of motion for a small rigid sphere in a non-uniform flow. *Phys. Fluids* **26**, 883–889.

MEI, R., ADRIAN, R. J. & HANRATTY, T. J. 1991 Particle dispersion in isotropic turbulence under Stokes drag and Basset force with gravitational settling. *J. Fluid Mech.* **225**, 481–495.

PAI, M. G. & SUBRAMANIAM, S. 2006 Modeling interphase turbulent kinetic energy transfer in Lagrangian–Eulerian spray computations. *Atomiz. Sprays* **16** (7), 807–826.

PAI, M. G. & SUBRAMANIAM, S. 2007 Modeling droplet dispersion and interphase turbulent kinetic energy transfer using a new dual-timescale Langevin model. *Intl J. Multiphase Flow* **33** (3), 252–281.

PAI, M. G. & SUBRAMANIAM, S. 2009 A comprehensive probability density function formalism for multiphase flows. *J. Fluid Mech.* **628**, 181–228.

PASCAL, P. & OESTERLÉ, B. 2000 On the dispersion of discrete particles moving in a turbulent shear flow. *Intl J. Multiphase Flow* **26**, 293–325.

POPE, S. B. 1985 PDF methods for turbulent reactive flows. *Prog. Energy Combust. Sci.* **11**, 119–192.

POPE, S. B. 2000 *Turbulent Flows*. Cambridge University Press.

POPE, S. B. 2002 Stochastic Lagrangian models of velocity in homogeneous turbulent shear flow. *Phys. Fluids* **14** (5), 1696–1702.

POZORSKI, J. & MINIER, J.-P. 1999 Probability density function modeling of dispersed two-phase turbulent flows. *Phys. Rev.* E **59** (1), 855–863.

SAWFORD, B. L. & YEUNG, P. K. 2001 Lagrangian statistics in uniform shear flow: direct numerical simulation and Lagrangian stochastic models. *Phys. Fluids* **13**, 2627.

SIMONIN, O. 1996a Continuum modeling of dispersed turbulent two-phase flows. Part 1. General model description. *Tech. Rep.* Lecture Series. Von Kármán Institute of Fluid Dynamics.

SIMONIN, O. 1996b Continuum modeling of dispersed turbulent two-phase flows. Part 2. Model predictions and discussion. *Tech. Rep.* Lecture Series. Von Kármán Institute of Fluid Dynamics.

SNYDER, W. H. & LUMLEY, J. L. 1971 Some measurements of particle velocity autocorrelation functions in a turbulent flow. *J. Fluid Mech.* **48**, 41–71.

SQUIRES, K. D. & EATON, J. K. 1991 Measurements of particle dispersion obtained from direct numerical simulations of isotropic turbulence. *J. Fluid Mech.* **226**, 1–35.

SUNDARAM, S. & COLLINS, L. R. 1999 A numerical study of the modulation of isotropic turbulence by suspended particles. *J. Fluid Mech.* **379**, 105–143.

TEN CATE, A., DERKSEN, J. J., PORTELA, L. M. & VAN DEN AKKER, H. E. A. 2004 Fully resolved simulations of colliding monodisperse spheres in forced isotropic turbulence. *J. Fluid Mech.* **519**, 233–271.

TRUESDELL, G. C. & ELGHOBASHI, S. 1994 On the two-way interaction between homogeneous turbulence and dispersed solid particles. II. Particle dispersion. *Phys. Fluids* **6** (3), 1405–1407.

WELLS, M. R. & STOCK, D. E. 1983 The effects of crossing trajectories on the dispersion of particles in a turbulent flow. *J. Fluid Mech.* **136**, 31–62.

XU, Y. & SUBRAMANIAM, S. 2006 A multiscale model for dilute turbulent gas–particle flows based on the equilibration of energy concept. *Phys. Fluids* **18**, 033301.

XU, Y. & SUBRAMANIAM, S. 2007 Conservative interphase turbulent kinetic energy transfer in particle-laden flows. *Phys. Fluids* **19**, 085101.

XU, Y. & SUBRAMANIAM, S. 2010 Effect of particle clusters on carrier flow turbulence: A direct numerical simulation study. *Flow Turbul. Combust.* **85**, 735–761.

YEUNG, P. K. & POPE, S. B. 1989 Lagrangian statistics from direct numerical simulations of isotropic turbulence. *J. Fluid Mech.* **207**, 531–586.

YUSOF, M. J. 1996 Interaction of massive particles with turbulence. PhD thesis, Cornell University.